AFRL-OSR-VA-TR-2015-0172

SENSING RANDOM ELECTROMAGNETIC FIELDS AND APPLICATIONS

Aristide Dogariu
UNIVERSITY OF CENTRAL FLORIDA

06/23/2015
Final Report

Air Force Research Laboratory
AF Office Of Scientific Research (AFOSR)/ RTB
Arlington, Virginia 22203
Air Force Materiel Command

Report Documentation Page

Form Approved
OMB No. 0704-0188

1. REPORT DATE	2. REPORT TYPE	3. DATES COVERED
23 JUN 2015		**01-05-2010 to 30-04-2015**

4. TITLE AND SUBTITLE	5a. CONTRACT NUMBER
Sensing Random Electromagnetic Fields and Applications	5b. GRANT NUMBER
	5c. PROGRAM ELEMENT NUMBER
6. AUTHOR(S)	5d. PROJECT NUMBER
	5e. TASK NUMBER
	5f. WORK UNIT NUMBER
7. PERFORMING ORGANIZATION NAME(S) AND ADDRESS(ES) **University of Central Florida,,4000 Central Florida Blvd.,Orlando,,FL,32816**	8. PERFORMING ORGANIZATION REPORT NUMBER
9. SPONSORING/MONITORING AGENCY NAME(S) AND ADDRESS(ES)	10. SPONSOR/MONITOR'S ACRONYM(S)
	11. SPONSOR/MONITOR'S REPORT NUMBER(S)

12. DISTRIBUTION/AVAILABILITY STATEMENT
Approved for public release; distribution unlimited

13. SUPPLEMENTARY NOTES

14. ABSTRACT

Random electromagnetic fields (REF) exist in all forms and one common origin is a result of the interaction of coherent fields with randomly inhomogeneous media. This coherent light-matter interaction is a complex interference process leading to fields with strong fluctuations in intensity, fields that are most commonly known as speckle. A simple way to describe the intensity speckles is to consider the superposition of waves originating from discrete centers as a result of scattering. Different scattering regimes may vary from single scattering specific to most surface scattering to different degrees of multiple scattering characteristic to the interaction with three-dimensionally disordered media. When one single polarization component is analyzed, i.e. when the speckle field is measured through a polarizer, the intensity contrast often reaches unity. This is the case of the so-called fully developed speckle pattern, a manifestation of interference between a large numbers of wavelets with uniformly distributed random phases.

15. SUBJECT TERMS

16. SECURITY CLASSIFICATION OF:			17. LIMITATION OF ABSTRACT	18. NUMBER OF PAGES	19a. NAME OF RESPONSIBLE PERSON
a. REPORT	b. ABSTRACT	c. THIS PAGE			
unclassified	**unclassified**	**unclassified**	**Same as Report (SAR)**	**43**	

REPORT DOCUMENTATION PAGE

Form Approved
OMB No. 0704-0188

1. REPORT DATE *(DD-MM-YYYY)*	2. REPORT TYPE	3. DATES COVERED *(From - To)*
17-07-2015	Final Performance	01-05-2010 to 30-04-2015

4. TITLE AND SUBTITLE
SENSING RANDOM ELECTROMAGNETIC FIELDS AND APPLICATIONS

5a. CONTRACT NUMBER

5b. GRANT NUMBER
FA9550-10-1-0190

5c. PROGRAM ELEMENT NUMBER

6. AUTHOR(S)
Aristide Dogariu

5d. PROJECT NUMBER

5e. TASK NUMBER

5f. WORK UNIT NUMBER

7. PERFORMING ORGANIZATION NAME(S) AND ADDRESS(ES)
UNIVERSITY OF CENTRAL FLORIDA
4000 CNTRL FLORIDA BLVD
ORLANDO, FL 32816 US

8. PERFORMING ORGANIZATION REPORT NUMBER

9. SPONSORING/MONITORING AGENCY NAME(S) AND ADDRESS(ES)
AF Office of Scientific Research
875 N. Randolph St. Room 3112
Arlington, VA 22203

10. SPONSOR/MONITOR'S ACRONYM(S)
AFOSR

11. SPONSOR/MONITOR'S REPORT NUMBER(S)

12. DISTRIBUTION/AVAILABILITY STATEMENT
A DISTRIBUTION UNLIMITED: PB Public Release

13. SUPPLEMENTARY NOTES

14. ABSTRACT
Random electromagnetic fields (REF) exist in all forms and one common origin is a result of the interaction of coherent fields with randomly inhomogeneous media. This coherent light-matter interaction is a complex interference process leading to fields with strong fluctuations in intensity, fields that are most commonly known as speckle. A simple way to describe the intensity speckles is to consider the superposition of waves originating from discrete centers as a result of scattering. Different scattering regimes may vary from single scattering specific to most surface scattering to different degrees of multiple scattering characteristic to the interaction with three-dimensionally disordered media. When one single polarization component is analyzed, i.e. when the speckle field is measured through a polarizer, the intensity contrast often reaches unity. This is the case of the so-called fully developed speckle pattern, a manifestation of interference between a large numbers of wavelets with uniformly distributed random phases.

15. SUBJECT TERMS
AND, APPLICATIONS

16. SECURITY CLASSIFICATION OF:			17. LIMITATION OF ABSTRACT	18. NUMBER OF PAGES	19a. NAME OF RESPONSIBLE PERSON
a. REPORT	b. ABSTRACT	c. THIS PAGE			Aristide Dogariu
U	U	U	UU		19b. TELEPHONE NUMBER *(Include area code)* 407-823-6839

Standard Form 298 (Rev. 8/98)
Prescribed by ANSI Std. Z39.18

To: **Dr. Julie Moses**

Subject: **Final Report**

Contract/Grant Title**: Sensing Random Electromagnetic Fields and Applications**

Contract/Grant #: **FA95501010190**

PI: **Aristide Dogariu**

Content:

A. Stochastic Electromagnetics for Sensing

A1 Complex degree of mutual polarization in randomly scattered fields

Random electromagnetic fields (REF) exist in all forms and one common origin is a result of the interaction of coherent fields with randomly inhomogeneous media. This coherent light-matter interaction is a complex interference process leading to fields with strong fluctuations in intensity, fields that are most commonly known as speckle. A simple way to describe the intensity speckles is to consider the superposition of waves originating from discrete centers as a result of scattering. Different scattering regimes may vary from "single scattering" specific to most surface scattering to different degrees of multiple scattering characteristic to the interaction with three-dimensionally disordered media. When one single polarization component is analyzed, i.e. when the speckle field is measured through a polarizer, the intensity contrast often reaches unity. This is the case of the so-called fully developed speckle pattern, a manifestation of interference between a large numbers of wavelets with uniformly distributed random phases. This is a rather universal behavior present in scattering from a variety of media ranging from metallic rough surfaces to diffusive materials. However, the distribution of polarization states in REF is much richer and non-universal properties are to be expected. Most importantly, it is anticipated that the polarization properties of REF corresponding to different scatting regimes will depend greatly on the strength of the scattering process. For instance, it is likely that when the wave interaction is dominated by single scattering processes, a fully developed speckle pattern will occur but the REF polarization will strongly resemble the incident state of polarization. On the other hand, when the interaction is subject to strong multiple scattering, the scattered field remains locally fully polarized but its state of polarization will vary from point to point. When the scattering process is completely diffusive, universal distributions emerge for the polarization parameters. It is therefore of interest to examine in detail the relation between the degree (order) of scattering and the polarization properties of the resulting REF.

Usually, the formation of speckle is described as a scalar process in terms of a random walk of complex phasors. The addition of a large number of random phasors with different lengths and directions leads to a scattered intensity pattern which has a negative exponential probability distribution. If the initial source of radiation is fully polarized and coherent, the wave interacting with a non-absorbing medium remains coherent and fully polarized at each point in space. As mentioned in the introduction, in a fully developed speckle, the global field is fully polarized, often arising from a strong single scattering process such as the interaction with a rough metallic surface. In cases in which the interaction with the medium is a multiple scattering process, the individual speckles remain locally fully polarized although globally the field becomes partially polarized. Even a completely globally "unpolarized" speckle pattern is locally fully polarized.

A simple experiment was designed to image the REF at the surface of scattering media in a backscattering geometry. The samples were illuminated with a large, linearly polarized beam from a laser with a wavelength of 488nm and the surface was imaged onto a CCD. At the surface of the medium, the speckles are of the order of the wavelength and, in order to fully resolve them, they were magnified about ninety times to about 80μm in size. We used a number of sample media with varying degrees of rough surfaces and volume scattering. Figure 1 illustrates several experimentally obtained REF corresponding to a rough metallic surface (A) and three diffuse

volume scattering media characterized by different transport mean free paths: a thin kaolin based diffuse coating (B), a cellulose membrane (C), and a polyvinylidene fluoride membrane (D).

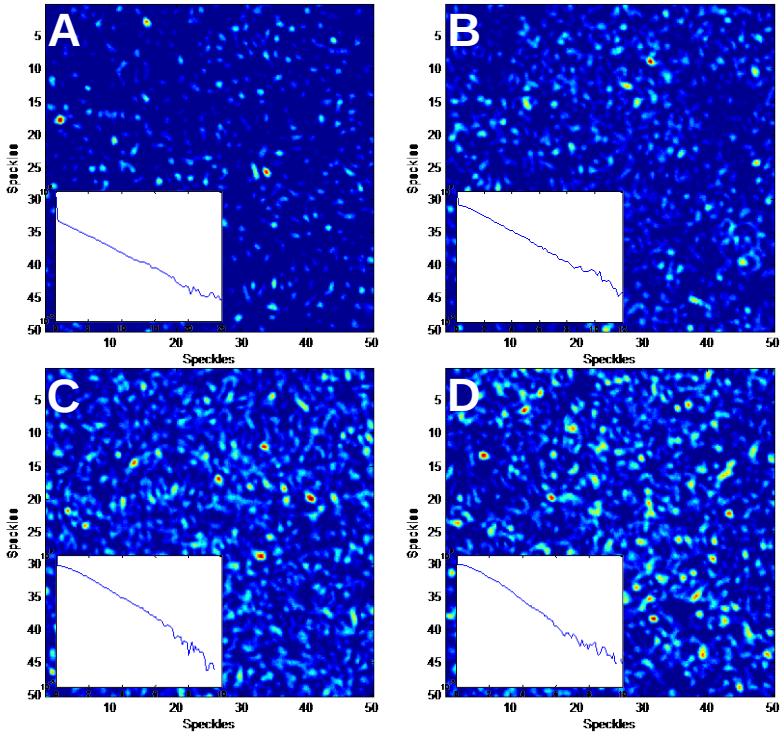

Fig. 1. Intensity patterns scattered from four different media: a rough metallic surface (A), a thin kaolin based diffuse coating (B), a cellulose membrane (C), and a polyvinylidene fluoride membrane (D). The insets show the corresponding $\log(p(I/\langle I\rangle))$ vs $I/\langle I\rangle$ distributions.

As can be seen, in spite of their different origins, the random fields illustrated in Fig. 1 are all developed speckle patterns as demonstrated by the probability density functions of normalized intensities shown in the corresponding insets; the $p(I/\langle I\rangle)$ distributions all manifest negative exponential decays. In addition, from the intensity distributions one can evaluate the second order intensity correlations $\langle I(r)I(r+\rho)\rangle$, i.e. the average speckle size. In all cases shown in Fig. 1, the average speckle size is approximately the wavelength of light. As such, one can conclude that both 1st and 2nd order intensity correlations are quite similar in all cases in spite of the fact that the REFs are generated by scattering on quite different random media. This means that the intensity statistics is insufficient to discriminate between REFs that are generated via different regimes of scattering.

In contrast, it is known that the polarization is more robust and resistant to random fluctuations. For instance, in single scattering from rough surfaces, the state of polarization is maintained. As the contribution of multiple scattering increases, the wave depolarizes, usually over length scales greater than the transport mean free path. Therefore, it is expected that the correlation between polarization states at the surface should be indicative of the scattering level within the random medium.

A2 Scale dependent degree of polarization

Let us now examine the vectorial nature of the scattered fields and inspect their polarization properties. A rotating quarter-wave plate was inserted in the imaging path of the experimental setup and a subsequent Fourier analysis provided the full Stokes vector in each pixel. The spatially resolved polarimetric description of the REF can subsequently be analyzed in different ways. A common measure of polarization is the degree of polarization (DoP) $P(\bar{r}_i) = \sqrt{S_1^{\,2}(\bar{r}_i) + S_2^{\,2}(\bar{r}_i) + S_3^{\,2}(\bar{r}_i)} / S_0(\bar{r}_i)$

where

$$S_1(r) = E_x^*(r)E_x(r) - E_y^*(r)E_y(r)$$
$$S_2(r) = E_x^*(r)E_y(r) - E_y^*(r)E_x(r) \quad .$$
$$S_3(r) = i\left(E_x^*(r)E_y(r) - E_y^*(r)E_x(r)\right)$$

As can be seen, the DoP is actually a 4th-order field correlator describing the properties of the electric field at point *r*. Practically, one has access to an ensemble of different polarization states collected over a certain area and a scale dependent effective DoP can be estimated as $\overline{P}_A(r) = \sqrt{\int_A S_1^{\,2} dr + \int_A S_2^{\,2} dr + \int_A S_3^{\,2} dr} / \int_A I dr \cdot$

The scale dependent DoP in Eq. (3) approaches zero when the ensemble of polarization states are randomly distributed over the Poincare sphere as illustrated in Fig. 2. Of course, a strong multiple scattering interaction leads to an overall depolarized scattered field when the DoP is evaluated over a large scale. We emphasize that this depolarization only occurs in the global sense, as the resulting scattered light forms individually fully polarized speckles. The depolarization measurement can be viewed as a "center of mass" estimation, where the polarization of the average state lies within the sphere as seen in Fig. 2b.

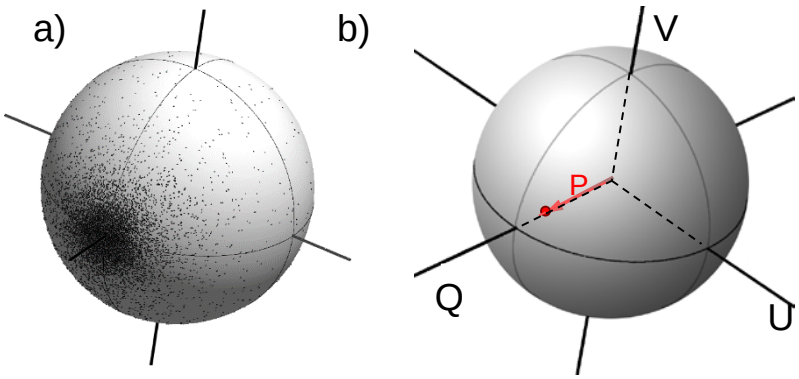

Fig. 2. a) Distribution of polarization states on the Poincare sphere. b) Both the average state of polarization and the degree of polarization are ensemble properties of the distribution of polarization states.

Results of calculations of scale-dependent DoP are presented in Fig. 3. As we increase the size of the area over which the estimation is performed, the DoP value eventually reaches saturation. The error bars in Fig 3 were calculated using one hundred starting points for each size of analysis area. Their values reflect the fact that even if each speckle is fully polarized, $\overline{P}_A(r)$ varies significantly when only examining a small number of speckles. As evident, there are two

factors associated with the DoP scale dependence: the saturation level and the associated decay length. It is quite clear that the saturation levels can be quite different. For the samples illustrated here, the DoP saturation values are 0.97, 0.49, 0.32, and 0.32 +/- 0.02 for samples A, B, C, and D, respectively. Different saturation levels indicate different levels of global depolarization due to scattering: the higher the level of multiple scattering the lower the value of the corresponding degree of global polarization of the scattered field. However, the two membrane samples (C and D) show very similar DoP saturation values yet they have completely different material structures. In this case the DoP value is insufficient to discriminate between different levels of multiple scattering.

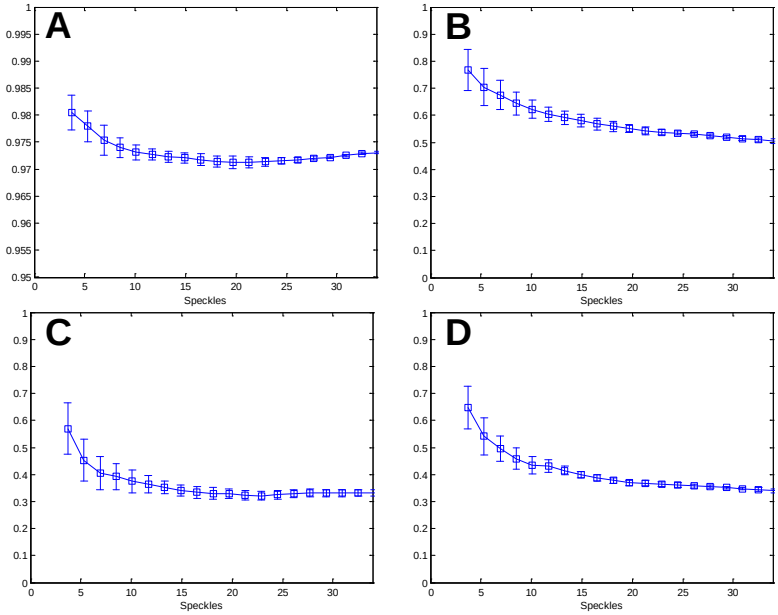

Fig. 3. The DoP calculated over an increasing integration area averaged over 100 integration centers. The error bars indicate the DoP standard deviation calculated for each integration area. Note that the y-scale in A is 0.95-1.0 while it is 0-1.0 for panels B, C, and D.

The DoP decay length represents the spatial scale at which saturation is reached. Although the media examined here have different saturations, they all have similar decay lengths measuring about 15 intensity speckles. It appears that this decay length is an associated ensemble quantity that ignores any underlying material discrepancies. The DoP is a basic yet incomplete way to describe the polarization properties of REF. As mentioned before, the DoP is evaluated based on 4^{th}-order field correlations representative for the properties of a field at one spatial location. It is also an ensemble quantity, averaged over many spatial locations, and therefore it loses any information about spatial distribution of polarization states, i.e. the shape of the distribution of states on the Poincare sphere. For instance, there are many different REF that can be characterized by the same value of the global DoP. In the following we will examine a more refined, two-point descriptor of the polarization properties of a random field.

A3 Two point polarization correlations

Another possibility to evaluate higher-order field correlations in REF is to quantify the variability between the members of the ensemble of measurement points and a chosen reference. The measure for this is the complex degree of mutual polarization (CDMP). The magnitude of the CDMP measures the polarization similarity between two points, r_i and a reference $r_{0,}$ and under the assumption of a fully correlated and locally fully polarized field, it is defined as

$$V^2(r_i, r_0) = \frac{\left(E_x^*(r_i)E_x(r_0) + E_y^*(r_i)E_y(r_0)\right)^2}{\left(\left|E_x(r_i)\right|^2 + \left|E_y(r_0)\right|^2\right)\left(\left|E_x(r_i)\right|^2 + \left|E_y(r_0)\right|^2\right)}.$$

As such, CDMP measures the distance between two points (states of polarization) on the Poincare sphere; orthogonal states, opposite to each other on the Poincare sphere, have an associated CDMP value of zero. The CDMP reflects the shape of the distribution of states on the Poincare sphere in contrast to the DoP, which is a measure of the location of the center of mass of the distribution. CDMP quantifies the spatial distribution of states by comparing the Stokes vectors in each point to a common reference. Recently, similar estimations of REF properties permitted to detect local non-stationarities such as the presence of a weak localization phenomenon.

It is important to note that CDMP is not an ensemble quantity and it can be calculated while maintaining spatial information. In Fig 4 we show the spatial distribution of the REFs in Fig. 1 but this time encoded in the CDMP values calculated with respect to the constant state of polarization of the incident field.

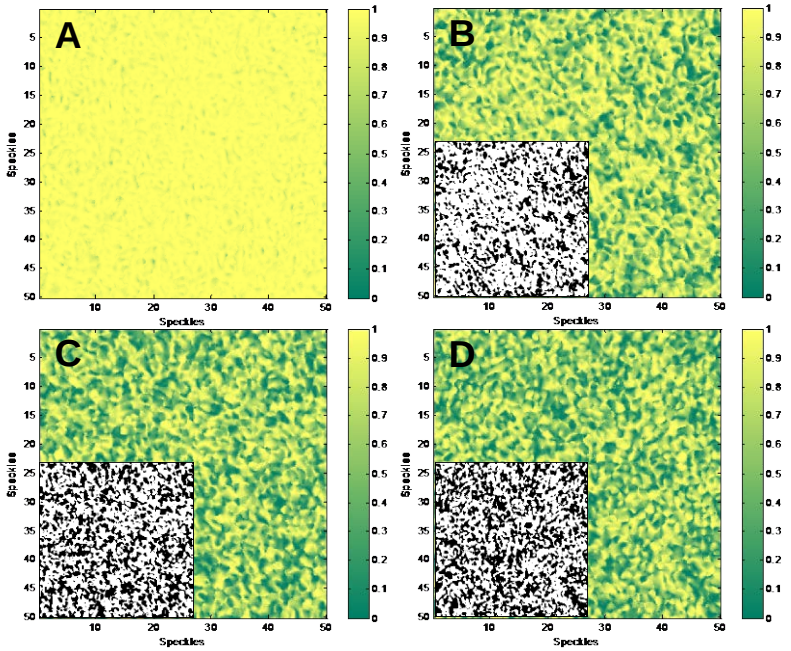

Fig. 4. CDMP maps of the REF in Fig. 1 calculated with respect to incident state of polarization. Insets show binary images of corresponding maps thresholded at CDMP=0.5.

As can be seen, the CDMP maps provide information about the similarity of polarization states in the REF. The rough metallic surface, sample (A) in Fig. 4, exhibits strong single scattering and as a result most of the scattered field is in the same state of polarization as the incident one; the CDMP is almost uniformly unity as a result of the strong spatial correlation of the polarization. As the level of multiple scattering increases, the spatial correlation of the CDMP maps reduces as seen for samples B, C, and D.

To assess quantitatively the differences between the CDMP maps, one can examine the probability density functions (PDF) corresponding to the distributions of CDMP values across the image. As can be seen in Fig. 5, different distributions are found for the CDMP maps shown in Fig 4. Clearly, the PDFs evolve from being peaked around unity in the case of single scattering (rough surface A) to a more uniform distribution corresponding to the higher order multiple scattering processes in volume scattering media. An interesting observation can be made in regard to samples C and D. Even though the REF scattered by these media have almost the same global degree of polarization, the PDFs of their corresponding CDMP maps are noticeably different. This can be interpreted as different coverage on the Poincare sphere corresponding to similar centers of mass. Being a local 4^{th}-order field correlation, CDMP preserves the spatial information and distinguishes between different underlying field distributions that have similar average properties.

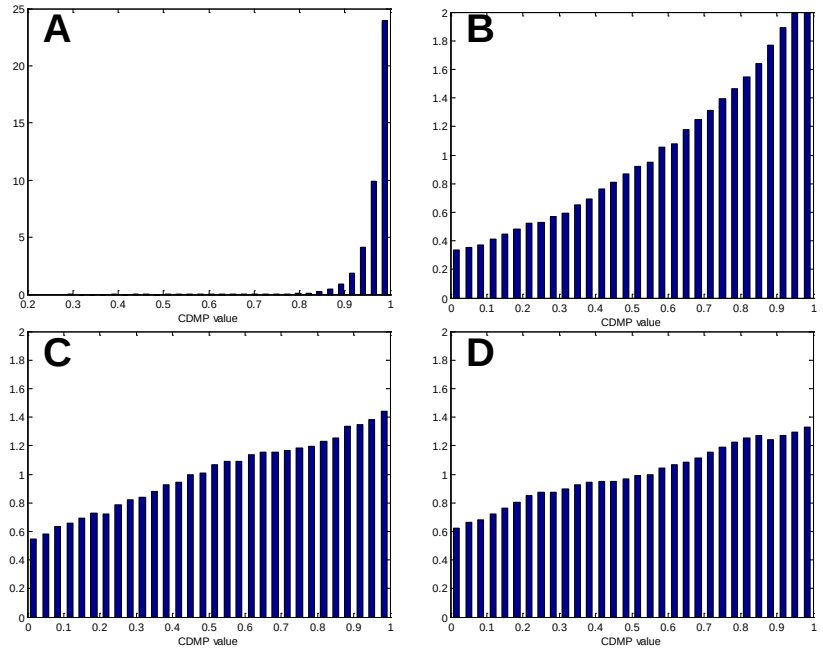

Fig. 5. Probability density functions for the CDMP distribution maps shown in Fig. 4.

We note that for a fully diffusive process of wave interaction all polarization states are equally probable and a uniform PDF is to be expected. The slight increase of the probability density towards higher CDMP values means that the diffusive scattering behavior has not been reached. In the present case this is a consequence of the backscattering geometry where the low-order scattering events are always dominant.

Let us now turn our attention to the spatial characterization of the CDMP maps in Fig. 4. As can be seen, these maps reveal areas of more uniform polarization. One can interpret theses

areas of spatial variation of the CDMP values as determining some sort of polarization or CDMP "speckles". This spatial correlation over the CDMP maps is more obvious in the binary images included as insets in Fig. 4. The binary distributions were obtained by thresholding all the points having a CDMP value greater than 0.5. The field in A is clearly dominated by single scattering, where the incident state of polarization is largely maintained. In the binary images corresponding to the other samples, the different extent of clearly defined areas with similar polarization is evident, which can be understood as different levels of spatial correlations between the CDMP values. This is akin to defining an average size of the CDMP "speckle".

When considering the distributions in the binary map shown in Fig. 4B, we found that the average size of correlated areas is about 5.3 times larger than the average size of an intensity speckle. The size of the correlation areas clearly decreases for samples C and D where it is 3.3 and 3.0 intensity speckles, respectively. Of course, the number of clusters and their size depend upon the threshold level. As the threshold decreases, the total number of points that lay above this level increases and the size of these correlated areas increases as shown in Fig. 6. However, the areas increase at different rates as clearly seen in Fig. 6, indicating different structures in the CDMP maps and, moreover, a distinctive dependence on the level of scattering in each sample. We should reiterate that both the distribution of CDMP values in Fig. 5 and the extent of the two-dimensional CDMP correlations in Fig. 6 are obtained from one single realization of the random fields shown in Fig. 4. Thus, this analysis constitutes the point and the point-pair characterization of the polarization properties of the scattered electromagnetic field in a manner similar to the intensity distribution $p(I)$ and the average intensity-intensity correlation $\langle I(r)I(r+R)\rangle$ in a scalar speckle pattern.

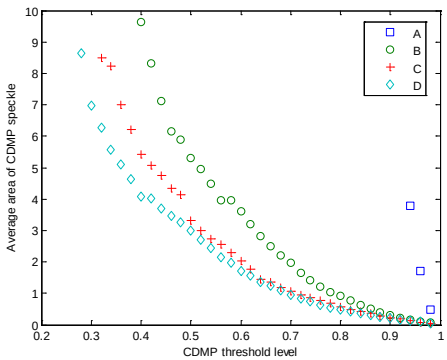

Fig. 6. Size of CDMP speckle in units of intensity speckles as a function of CDMP threshold level. Different decay rates are evident for the four samples examined.

There is an intimate dependence between the medium's structure and the polarimetric properties of the scattered field and, therefore, one can anticipate that the distribution of polarization states and their spatial correlation in a REF should reflect some of the morphological properties of the scattering media. Being a measure of polarization similarity at different spatial locations, the size of the CDMP speckle reflects the extent of the interaction volume necessary for the wave to depolarize, or, in other words, to lose memory of its initial polarization state. In a specific geometry, the magnitude of this characteristics length scale depends on the number of transport mean free paths. Therefore, scattering media characterized by small values of l* are also expected to generate, at their surface, scattered fields with smaller value of the CDMP speckles. This is exactly what our experiments show; the lowest value of the CDMP speckle corresponds to the strongest scattering in sample D. Remarkably, one single realization of the scattering

process is sufficient to provide information similar to that acquired through an ensemble average measurement.

A4 Identifying non-stationarities in random fields

There is little to say about the wave-matter interaction when the resulting random field obeys Gaussian statistics. However, there are instances in which the assumptions of Gaussianity, stationarity, and ergodicity are not fully satisfied. For instance, specific spatial correlations between sources can produce non-stationary statistics in a speckle field. In this context, one intriguing situation is that of the weak localization of waves in reflection. When a plane wave is incident upon a random medium, the probabilities of any given scattering path and its time reversed pair are equal. In the exact backscattering direction, all such pairs interfere constructively. The location of this maximal interference is independent of a particular path or realization, leading to a "coherent" effect known as enhanced backscattering (EBS). Because of this phenomenon, the intensity distribution is a random process that is spatially non-stationary; its mean value varies with the spatial location. EBS is typically observed as the result of an ensemble average over many realizations of the interaction between a coherent wave and a multiple scattering medium. This average is usually performed by changing the medium's configuration but it can also be achieved through wavelength diversity. Of course, the presence of an enhancement in the backscattering direction is masked by the random intensity distribution that constitutes the speckle pattern. The existence of this spatial non-stationarity however should be present in each realization of the interaction between a coherent wave and a random medium and one can ask the question: is this information retrievable without having access to the ensemble average? To answer it, we will inspect such random field distributions by examining their statistical properties beyond the second-order field correlations.

Given a spatial non-stationarity, it follows that the field distribution is non-ergodic. Specifically, as the ensemble average depends on location, it is not possible for the spatial average to equal the ensemble average at every point. However, in practice it may be possible to treat the field as *locally, spatially ergodic*. That is to say that the spatial average over some region about a given point may recover the ensemble average value at that point. However, the concept of local spatial ergodicity raises a number of issues regarding the length scales of the field distribution, the field measurement, and its characterization. For instance, the region of spatial averaging must be sufficiently large to provide reasonable statistics, and yet not so large as to wash out the spatial non-stationarity. We will discuss these aspects in the context of different methods for characterizing such field distributions. Based on the assumption of local ergodicity over certain spatial domains, we will examine two different methods that may be capable of discerning ensemble-like information from one single realization of the random field. The simplest approach to duplicate the ensemble intensity average is to take a moving spatial intensity average. The effective intensity $\bar{I}$ at a point r calculated for a spatial subdomain A can be defined as $\bar{I}_A(r) = \frac{1}{\|A\|}\int_A I(r+r_0)dr_0$ where $I(r) = E_x^*(r)E_x(r) + E_y^*(r)E_y(r)$. As the phenomenon of interference between time reversed paths is polarization dependent, another possibility would be to examine polarimetric quantities [6]. Specifically, the constructive interference relies on polarization similarity, that can be gauged by the degree of polarization estimated over a spatial subdomain A [7]. This effective degree of polarization $\overline{P}$ can be defined as

$$\overline{P}_A(r) = \frac{\sqrt{\int_A S_1^2 dr + \int_A S_2^2 dr + \int_A S_3^2 dr}}{\int_A I dr}, \qquad \text{where} \quad \begin{aligned} S_1(r) &= E_x^*(r)E_x(r) - E_y^*(r)E_y(r) \\ S_2(r) &= E_x^*(r)E_y(r) - E_y^*(r)E_x(r) \\ S_3(r) &= i\left(E_x^*(r)E_y(r) - E_y^*(r)E_x(r)\right) \end{aligned}.$$

It is interesting to note that, unlike the effective intensity, this quantity inherently involves fourth-order field correlations, and as such, can be expected to be more sensitive to fluctuations in the field distribution.

Both parameters can be used to encode the spatial distribution of a random field (a speckle-like image) by producing an average over a subdomain *A* and then associating that value with the corresponding location in the initial field. However, the choice for the size of such a subdomain is arbitrary and most importantly, introduces an artificial length scale. In other words, one may find an appropriate size of the subdomain for which the non-stationarity can be revealed but the size of such subdomain is not known a priori; moreover, this choice may depend on characteristic length scales of the specific problem. These length scales are the physical extent of the non-stationarity and the overall size of the available data, i.e. the largest scale length in the random field. In fact, the existence of an appropriate size of the subdomain is inherently tied to the existence of a spatial non-stationarity.

To avoid having to find an optimum size of the subdomain that would reveal a specific non-stationarity, we examine another possible measure that is based on the recently introduced complex degree of mutual polarization (CDMP) of a random electromagnetic field. The magnitude of the CDMP measures the polarization similarity between two points, r_1 and r_2, in a random electromagnetic field. Under the assumption of a fully correlated and locally fully polarized field, the CDMP simplifies to

$$V^2(r_1, r_2) = \frac{\left(E_x^*(r_1)E_x(r_2) + E_y^*(r_1)E_y(r_2)\right)^2}{\left(E_x^*(r_1)E_x(r_1) + E_y^*(r_1)E_y(r_1)\right)\left(E_x^*(r_2)E_x(r_2) + E_y^*(r_2)E_y(r_2)\right)}.$$

This two-point measure does not rely upon the choice of an artificial subdomain, and as such, it can provide a direct measure of the length scale associated with a certain physical process. We emphasize that, as in the case of the effective degree of polarization, the CDMP parameter contains fourth-order correlations between field components. However, in this case field components at different spatial locations are involved. Thus, one expects even higher sensitivity to specific characteristics of a random field.

Using the CDMP definition one can calculate the CDMP spatial decay length $\mathcal{L}(r)$ by evaluating in each point *r* the decay of $\left|V^2(r, r+\delta r)\right|$ for increasing values of δr averaged azimuthally. For identically polarized fields, $\left|V^2(r, r+\delta r)\right|$ is unity, while for a uniformly random distribution of states of polarization $\left|V^2(r, r+\delta r)\right|$ averages to one half. After evaluating the CDMP decay length for each point, these values can be used to generate a completely new spatial representation where each point is encoded in its corresponding value of the CDMP decay length.

$$I(k_i, k_f) = I_0 + \sum_{l,m} \left|A_{lm}\right|^2 \cos(k_i + k_f) \bullet (r_l - r_m) + F(k_i, k_f),$$

where k_i and k_f are the wave vectors of the incident and scattered plane wave and A_{lm} represents the complex amplitude of the wave having r_l and r_m as the ending points of a multiple scattering trajectory inside the random medium [10, 11]. The second term in Eq. (6) represents the non-stationary component that upon ensemble averaging leads to a cone of enhanced intensity.

To test the different methods for locating the presence of non-stationarity, a typical EBS experiment was conducted. The setup, built around a continuous-wave laser operating at 488 nm and a cooled CCD array, was described earlier. In addition, a full polarimetric measurement was performed in each pixel of the resolved speckle using a rotating quarter-wave plate and subsequent Fourier analysis. In the experiments, a 2mm beam was incident on the sample and produced in the plane of the CCD a speckled field with an average size of the speckle of about 64μm. The sample was mounted on a spin plate that allowed observing single realizations of the scattered field as well as the corresponding ensemble average.

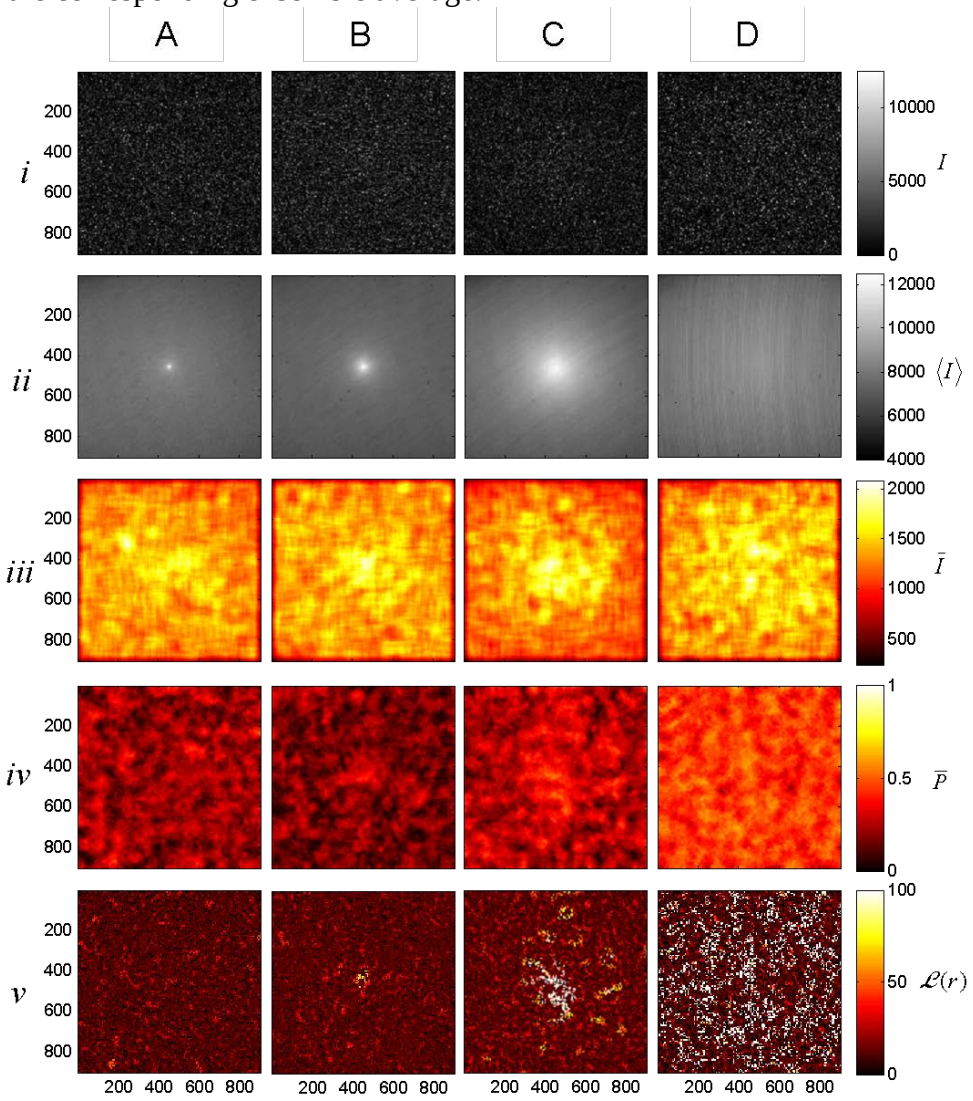

Fig. 7. Images corresponding to samples A, B, C, and D as described in the text. (i) single realization speckle intensity image, (ii) ensemble average, (iii) image encoded in the calculated effective intensity, (iv) image encoded in the calculated effective degree of polarization, (*v*) image encoded in the calculated polarization decay.

The scattering media used were different diffusing materials exhibiting minimal absorption. A large range of transport mean free paths, *l** values, was covered using different solid samples: (A) Suba IV™ polishing pad (Rodel), (B) Spectralon® (Labsphere), (C) Durapore™-HVLP filter

paper (Millipore), and (D) compressed TiO2 powder (DuPont). The scattering strengths of these samples are very different. From the widths of the corresponding EBS cones the estimated values of l^* were 40m, 20m, and 7m for samples A, B, and C respectively. For the TiO2 sample a scattering mean free path of approximately 1m was determined using optical path-length spectroscopy. The results of applying the analysis methods are summarized in Figure 7. The first two rows illustrate a typical realization of the random distribution of backscattered intensity and the corresponding result of the ensemble average, respectively. The familiar appearance of a speckle field (first row) can be observed for all samples, and as can be seen, no sample specific information is practically available As a result of the ensemble average on the other hand, the extent of the enhanced intensity may provide means to discriminate between the different structures as can be seen in the second row. However, this ability is restricted by the spatial resolution and the extent of the accessible field (experimentally limited by the pixel size, numerical aperture, and number of pixels available). For instance, in the case of sample D, the ensemble average appears as an almost constant background. It is evident that in this case, one cannot conclude that the absence of a region of enhanced intensity is due to the peak being either too large or too narrow or simply because the recording is performed away from the backscattering direction.

In the third row, we present the results of calculating the effective intensity $\bar{I}$ over a region (square box) containing 61 x 61 pixels that was scanned across the entire speckle image shown in the first row. For each location, the value of $\bar{I}$ was attributed to the central pixel of the box. This method basically performs the subset average of intensity including many points instead of the ensemble average at the central point of this domain. Since the average intensity in the EBS region is higher than the background, one could also expect a similar effect in the effective intensity image. However, as can be seen in Figure 1, no such increase of intensity can be observed for samples A and D, but the reasons are quite different. In the case A, the non-stationarity cannot be resolved due to the size of the averaging box while in the case D, the process is simply stationary over the limited field available. A certain increased intensity is prevalent in the results for samples B and C where an intensity enhancement concentrated towards the center of the image may indicate the presence of a spatial non-stationarity.

In a completely similar manner, we have evaluated the effective degree of polarization $\overline{P}$ for a circular area with a radius of 31 pixels and the results are shown in the fourth row of Figure 7. Because the interference effects leading to the enhanced scattering rely upon polarization similarity, it is expected that regions with a higher degree of polarization should indicate the presence of EBS. This is indeed seen in our results where the $\overline{P}$ values around 0.5 clearly indicate the polarization similarity. It is interesting to note the increase in the $\overline{P}$ values from sample A to D and the existence of non-stationarities similar to the ones in the ensemble averages shown in the second row.

Of course, for a specific sample, both $\bar{I}$ and $\overline{P}$ images could have been optimized in order to illustrate the presence and identify the location of the enhancement peak. However, that would necessitate *a priori* knowledge about the extent of the non-stationarity in order to select an appropriate size of the averaging box as the size of the box is sample specific. This requirement can be avoided by using a higher-order polarimetric measure as demonstrated in the last row of Figure 1 where the images are encoded in the decay length of CDMP evaluated as described before. As can be seen, now there is an even stronger progression from left to right. As the size of the enhancement increases, the number of points having longer polarization decay lengths rises. Note

that there is no additional image processing involved and that the color coding indicates the actual decay length of CDMP measured in pixels. Samples B, C, and D all show strong spatial polarization correlations with increasing values of the polarization decay lengths. In the case A, there is simply not enough pixel resolution to evaluate a two-point characteristic such as CDMP. Perhaps the most interesting observation concerns the compressed TiO2 powder (sample D) which has a very small *l** leading to a large EBS cone. As pointed out before, in this case the ensemble average image cannot confirm the presence of a non-stationarity in the random distribution of intensity. Because of the limited angular resolution of the optical system, one cannot identify the presence of a region with enhanced intensity. However, the existence of the coherent enhancement is clearly visible in only one realization of the random speckle pattern when the higher-order two-point correlations of the field are examined. The high values of the CDMP decay length clearly indicate the existence of polarization similarities that are specific to EBS. Detailed features of the wave-matter interaction are therefore prevalent in one single realization of the emerging random field but their characterization requires access to higher-order statistics of the field.

Having access to polarimetric information across the spatial extent of the field allows building fourth-order joint statistical parameters. Specific features such as the presence of non-stationary points can now be identified in a random field. Furthermore, when using mutual polarization measures such as the CDMP decay length these features can be found without any prior knowledge of the spatial size of the non-stationarity. We have shown that fourth-order field correlations evaluated at pairs of points in a random electromagnetic field can reveal properties that until now were inferred only through an ensemble average.

The ability to identify a spatial non-stationarity using only one single realization of a random field opens up new avenues for using multiple light scattering techniques. Techniques using multi-order field correlations as a means of detecting spatial non-stationarities are not limited to solely polarimetric phenomena. As such, it should be possible to generalize our method to field correlations of arbitrary order, with a corresponding increase in the number of compared spatial locations. Furthermore, as we are relying upon field correlations, these analysis techniques are not necessarily specific to electromagnetic phenomena, and may find application in the measurement and characterization of any random field or process.

A5 Coherent superpostion of random electromagnetic fields

REFs can have different physical origins. For instance, depending on the type of interaction, there are different kinds of REFs that result from the coherent light scattering by randomly inhomogeneous media. Such fields are fully polarized locally but their global properties can vary from being fully polarized (same polarization state across the entire field) to being completely unpolarized (a uniform distribution of all possible polarization states). For instance, a strong multiply scattering medium will generate scattering fields that are globally unpolarized fields while uniformly polarized random fields can be the result of single scattering, surface scattering, and ballistic propagation through the medium or combinations of those. Of course, in addition to different polarization properties, these fields can also differ in their spatial coherence properties, and this diversity may be used to trace their actual physical origin.

In the following we will describe the superposition of two locally polarized fields: one field being gobally unpolarized $\mathcal{U} = E^U(r)\hat{e}(r)$ and the other one characterized by a uniform polarization state, $\mathcal{P} = E^P(r)\hat{e}_0$. If the fields are quasi-monochromatic and also mutually coherent, their addition leads to a new REF that is $E^R(r) = E^U(r)\hat{e}(r) + E^P(r)\hat{e}_0$. As mentioned before, a globally unpolarized

field can be regarded as the superposition of two uncorrelated components that are orthogonally polarized, one along *x* and the other one along *y*, for instance. This is an example of adding two independent fields in intensity, which reduces the optical contrast. The addition of more independent fields further reduces this contrast. However, when a fully polarized and coherent REF is added to the field $\mathcal{U}$, the optical contrast of $E^R(r)$ actually increases because the uniformly polarized component increases the magnitude of the field amplitude along a certain direction, thus biasing the overall polarization of $E^R(r)$. Not only does the addition of this coherent field increase the contrast, but it also increases the overall degree of polarization creating a partially polarized REF. This is similar to combining a completely unpolarized beam with a fully polarized one to create any partially polarized beam.

The globally unpolarized field ($\mathcal{U}$) can be modeled as a REF where the complex amplitude components E_x and E_y are both circular gaussian random functions. Each of these components can be represented as a sum of plane waves

$$E_\mu^U(\mathbf{r}) = \sum_j a_j \exp(i(k_j \cdot \mathbf{r} + \phi_{\mu,j}),\ \mu = x, y, \qquad (1)$$

where a_j is an amplitude, k_j are transverse wavenumbers, $\mathbf{r}$ is a position vector, and $\phi_{\mu,j}$ are uniformly random phases. When the field in Eq. (1) is added to a field uniformly polarized along *x*,

$$E_\mu^P(\mathbf{r}) = \sum_j b_j \exp(i(k_j \cdot \mathbf{r} + \phi_{\mu,j}), \qquad (2)$$

where b_j is a different set of amplitudes, there are several ways to characterize the properties of the resultant REF. One simple global measure is to compare the average intensities of the field $\mathcal{P}$ with the the average intensity in the total field $E^R(r)$. In our practical example, this ratio $\beta = \left\langle \left|E^P(r)\right|^2 \right\rangle / \left\langle \left|E^R(r)\right|^2 \right\rangle$ would indicate the strength of the scattering regime. For instance, for $\beta > 0.5$, the REF would favor the linearly polarized component. We note that this ratio of intensities relates to the global degree of polarization, $\overline{P}$, of the final REF, which is an ensemble quantity defined as

$$\overline{P}(\mathbf{r}) = \sqrt{\left\langle S_1(\mathbf{r})\right\rangle^2 + \left\langle S_2(\mathbf{r})\right\rangle^2 + \left\langle S_3(\mathbf{r})\right\rangle^2} \,/ \left\langle I(\mathbf{r})\right\rangle, \qquad (3)$$

where

$$\begin{aligned} S_1(\mathbf{r}) &= E_x^{R*}(\mathbf{r})E_x^R(\mathbf{r}) - E_y^{R*}(\mathbf{r})E_y^R(\mathbf{r}) \\ S_2(\mathbf{r}) &= E_x^{R*}(\mathbf{r})E_y^R(\mathbf{r}) - E_y^{R*}(\mathbf{r})E_x^R(\mathbf{r}) \\ S_3(\mathbf{r}) &= i\left(E_x^{R*}(\mathbf{r})E_y^R(\mathbf{r}) - E_y^{R*}(\mathbf{r})E_x^R(\mathbf{r})\right) \end{aligned} \qquad (4)$$

As can be seen, the strength of the linearly polarized component determines the partial polarization of the resulting field. As β continues to increase, $\overline{P}$ increases as well until unity saturation is reached.

Another characteristic of the resultant field is the extent of its field-field correlations. In addition to having different overall magnitudes and polarization characteristics, random fields may also have different field correlation lengths. In other words, the speckle sizes of the fields $\mathcal{U}$ and $\mathcal{P}$ can be different. The short-range correlation length for $\mathcal{U}$ can be defined as

$$\left\langle E^U(\mathbf{r})E^U(\mathbf{r}+\delta)\right\rangle_{\mathbf{r}} = f(\delta^U), \tag{5}$$

and it has the same value for both *x* and *y* field components. The unpolarized field can be caused by any number of strongly scattering media but, for the purpose of this paper, it is assumed that the unpolarized field is examined near its source and, therefore, the field correlation length is of the order of a wavelength [17,18]. The field correlation for the linearly polarized component,

$$\left\langle E_x^P(\mathbf{r})E_x^P(\mathbf{r}+\delta)\right\rangle_{\mathbf{r}} = f(\delta^P), \tag{6}$$

is of course only along *x*. This can result from the scattering from a rough surface, ballistic scattering, and other types of scattering that conserve the state of polarization. Along with the value of β, these two correlation lengths directly influence the correlation length of the resulting REF.

As mentioned before, β, $\overline{P}$, and the *f* factors in Eqs. (5) and (6) are all global properties, evaluated as ensemble averages. While $\overline{P}$ is indicative of the overlap between the fields $\mathcal{U}$ and $\mathcal{P}$, its value does not take into account the field correlation in the resulting REF. The correlation length on the other hand is a structural characteristic evaluated using a two-point property. As the resulting REF has different levels of partial polarization depending on the strength of $\mathcal{P}$, the polarization structure of the final REF is important to consider.

In the past, we demonstrated that a two-point polarization similarity measure such as the complex degree of mutual polarization (CDMP) can conveniently describe the spatial structure of polarization in a REF without requiring an ensemble average. In general, the CDMP factor measures the similarity between two polarization states and it ranges from zero when the two states are orthogonal to unity when the polarization states are identical. For the purpose of the present analysis, the CDMP is defined such that it measures the correspondence between the state of polarization at position *r* and a chosen reference polarization state:

$$\left|V^2(r)\right| = \frac{\left(E_x^{R*}(r)E_x^P + E_y^{R*}(r)E_y^P\right)^2}{\left(\left|E_x^R(r)\right|^2 + \left|E_y^R(r)\right|^2\right)\left(\left|E_x^P\right|^2 + \left|E_y^P\right|^2\right)}. \tag{7}$$

In Eq. (7), the reference is the polarization state of the field $\mathcal{P}$. Using this definition, one can generate a two-dimensional CDMP map corresponding to this specific state of reference polarization as can be seen in Fig. 1. This two-dimensional graphical representation of polarization "speckle" is characterized by spatial features with different sizes and spatial frequencies. Similarly to conventional intensity speckles, it is expected that these features will depend on the properties of $\mathcal{U}$ and $\mathcal{P}$. Of course, since the field $\mathcal{P}$ is in the same polarization state of the reference, its CDMP map would have a uniform value of one; the CDMP map of $\mathcal{U}$ on the other hand should be correlated over distances on the order of δ^U.

As a means to assess the spatial frequencies in these polarization maps, one can examine the power spectral density (PSD) defined as

$$P(\omega) = F\left\{\left|V^2(r)\right| * \left|V^2(r)\right|\right\}, \tag{8}$$

where $\left|V^2(r)\right| * \left|V^2(r)\right|$ represents the autocorrelation of a CDMP map. Because the analyzed REF is the superposition of two other fields that are mutually coherent, Eq. (8) can be further written as

$$P(\omega) = \bar{I}_1^2 p_1(\omega) + \bar{I}_2^2 p_2(\omega) + \bar{I}_1 \bar{I}_2 p_{12}(\omega) \qquad (9)$$

where

$$p_j(\omega) = F\left\{a_j^* a_j * a_j^* a_j\right\}, \quad j = 1, 2$$

$$p_{12}(\omega) = F\left\{2a_1^* a_1 * a_2^* a_2 + \left(a_1^* a_2 + a_2^* a_1\right) * \left(a_1^* a_2 + a_2^* a_1\right)\right\}, \qquad (10)$$

represent the power spectral densities of the individual components and the mixed (interference) term, respectively. In Eq. (10), a_1 and a_2 denote the individual, normalized *x* field components $E^P(r)/S_0(r)$ and $E^U(r)/S_0(r)$, respectively. The properties of the spatial distribution of polarization states across a REF relate to the power spectrum of the CDMP map in Eq. (9), which, in our case, depends on the specific values of β and δ^P. Of course, the information content of this power spectrum in Eq. (9) is richer than that provided by the value of $\overline{P}$, which is only a global average of point-like properties.

In general, any REF can be decomposed into a globally unpolarized and a uniformly polarized component. These two components have a relative strength β and are also characterized by their, possibly different, coherence lengths δ^U and δ^P. These characteristics influence the global properties of REF in different ways. For instance, the global degree of polarization $\overline{P}$ of the final REF depends only on the ratio β but is not influenced at all by δ^U or δ^P. The spatial properties of polarization on the other hand are determined by all these factors as can be seen in the power spectrum of the CDMP map in Eqs. (9) and (10). Because (i) the global degree of polarization $\overline{P}$ can be determined independently and (ii) the coherence length δ^U is known to be of the order of the wavelength, one can use the power spectrum of the CDMP map to determine the unknown correlation length δ^P of the polarized field component. In the following we will illustrate this procedure using systematic numerical simulations.

To illustrate some of the field properties resulting from the superposition of coherent REFs, a simple numerical simulation was performed. Using the plane wave decomposition in Eq. (1), plane waves originating from a circular array of source points with random phases were mapped onto an observation plane of 250 by 250 pixels. This creates a Gaussian random field originating from a beam with radius *r*, with a coherence length $\delta^{coh} = 3.83/(\kappa r)$. When $\kappa = 1$ and $r = 0.3$, the coherence length δ^U of the globally unpolarized field was set to be equal about 12 pixels in the observation plane. The uniformly polarized field was created in a similar manner using Eq. (2) in only one linear state of polarization. In addition, the spatial correlation length of this polarized field (δ^P) was controlled by adjusting the parameter *r* to produce different values that are larger than δ^U. These two random fields are then superposed coherently and the resulting intensity patterns are shown in Fig. 8 for the case where the coherence length of the polarized field is four times larger than the one of the unpolarized component, i.e. $\delta^P = 4\delta^U$. In this example, the intensity patterns in Figs. 1(a) and (b) are characterized by a ratio $\beta = 0.15$, which corresponds to a global degree of polarization $\overline{P} = 0.11$.

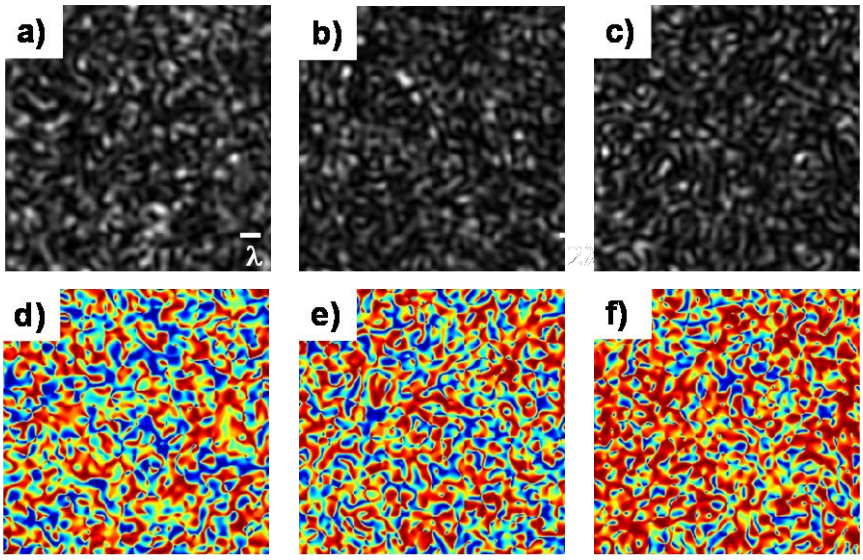

Fig. 8. Intensity speckle images of the superposition between an unpolarized field of coherence length δ^U and a polarized field characterized by: a) $\beta = 0.15$, $\delta^P = 4\delta^U$ b) $\beta = 0.15$, $\delta^P = \delta^U$ c) $\beta = 0.45$, $\delta^P = \delta^U$ and the corresponding CDMP maps for: d) $\beta = 0.15$, $\delta^P = 4\delta^U$ e) $\beta = 0.15$, $\delta^P = \delta^U$ and f) $\beta = 0.45$, $\delta^P = \delta^U$. Areas of blue and red correspond to CDMP values of 0 and 1, respectively. The values of $\beta = 0.15$ and $\beta = 0.45$ correspond to global degrees of polarization $\overline{P} = 0.11$ and $\overline{P} = 0.31$, respectively.

At such a low intensity ratio, adding an additional linearly polarized field has little impact and the resulting REF is almost globally unpolarized. As can be seen, even when the correlation length δ^P is four times larger than δ^U, there is practically very little change in the size of the final intensity speckles. However, when observing the CDMP maps, one can easily notice changes in the statistical nature of their structure. Even though the two REFs in Fig. 8(a) and 8(b) have the same global degree of polarization, there is a clear difference in the spatial frequency content of the corresponding CDMP maps as seen by the larger groupings of high CDMP values in Fig. 8(d).

The third speckle pattern in Fig. 8(c) corresponds to the situation where δ^P is equal to δ^U but the field $\mathcal{P}$ now has a greater amplitude, i.e. the ratio $\beta = 0.45$ and, correspondingly, $\overline{P} = 0.31$. As can be seen, the spatial frequency content in the CDMP map of Fig. 1(f) is similar to the one in Fig. 8(e) but now with a higher prominence of locations where $|V^2(r)| = 1$.

To get a quantitative description on how the correlation length of the field $\mathcal{P}$ affects the spatial distribution of polarization in the resulting REF, we have calculated the power spectral density of the CDMP maps resulting from the numerical procedure. An example is illustrated in Fig 9 for three cases corresponding to fields $\mathcal{P}$ having different correlation lengths and the same $\beta = 0.45$.

It is clearly seen that the characteristic shape of the curves in Fig. 9 appears to be composed of three different contributions. This is also described by Eq. (9) where the power spectral density contains three main terms that can be approximated by zero-mean Gaussians with different widths. The widths of these Gaussians are representative of the correlation lengths of the fields $\mathcal{P}$ and $\mathcal{U}$ while their magnitudes depend on the relative strengths of the fields (β). We have also fitted the

power spectral densities to the formulation in Eqs. (9) and (10) using the magnitudes I_1 and I_2 and the three Gaussian widths as fitting parameters. The results are included with continuous lines in Fig. 9. The first two terms correspond to the power spectral densities of the individual fields $\mathcal{P}$ and $\mathcal{U}$. Since the CDMP maps for the individual fields do not change with β and δ^P, the widths of the first two Gaussians also remain unchanged.

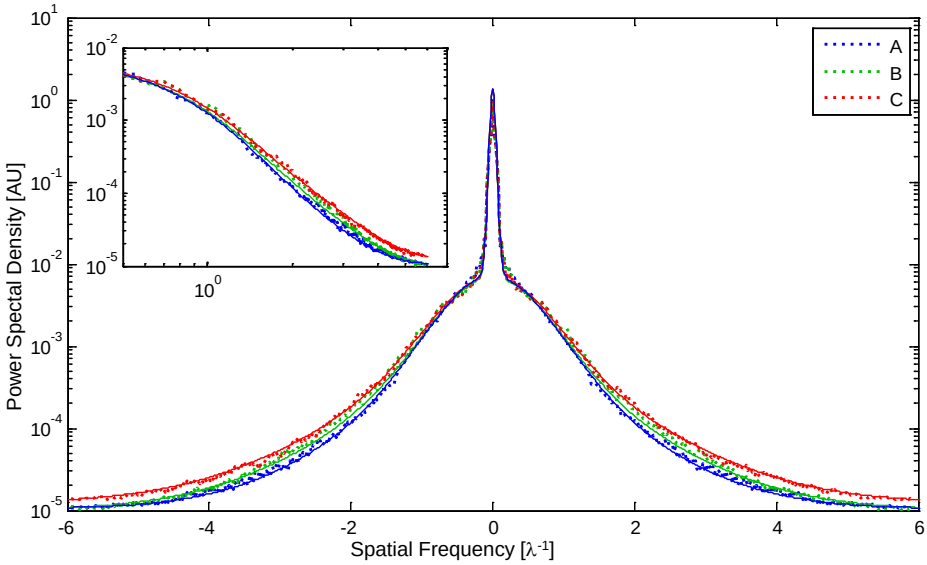

Fig. 9. The power spectral density of CDMP maps calculated for $\beta = 0.45$ and correlation lengths δ^P equal to A) $2\delta^U$, B) $4/3\delta^U$, and C) δ^U. Also shown with solid lines are the best fits with power spectrum dependence given in Eq. (9). The inset shows a log-log plot of the high spatial frequencies region.

In the specific case analyzed here, the first term, which is basically the PSD of the CDMP map with uniform unity value, has a small Gaussian width of 0.06 in our normalized units (the narrow central peak in Fig. 9). The second term represents the PSD corresponding to the unpolarized component and has a constant width of 0.9 due to the fixed correlation length δ^U. The third term in Eq. (9) describes the interference between the fields $\mathcal{P}$ and $\mathcal{U}$ with most of its contributions occurring in the high spatial frequency range. In the example presented in Fig. 9, only the width of this interference term and the magnitudes of the Gaussians depend on the characteristics of the interfering fields. However, because β is constant, all the magnitudes remain unchanged and only the width of the third component changes as δ^P varies. The contribution of this third term lies mostly in the high frequencies and can be fitted well with Gaussian function with widths of 3.6, 4, and 5.3 for the PSD labeled A, B, and C, respectively. As can be seen, as the correlation length of $\mathcal{P}$ decreases, the PSD width increases indicating that smaller spatial polarization features appear due to the interference between $\mathcal{P}$ and $\mathcal{U}$.

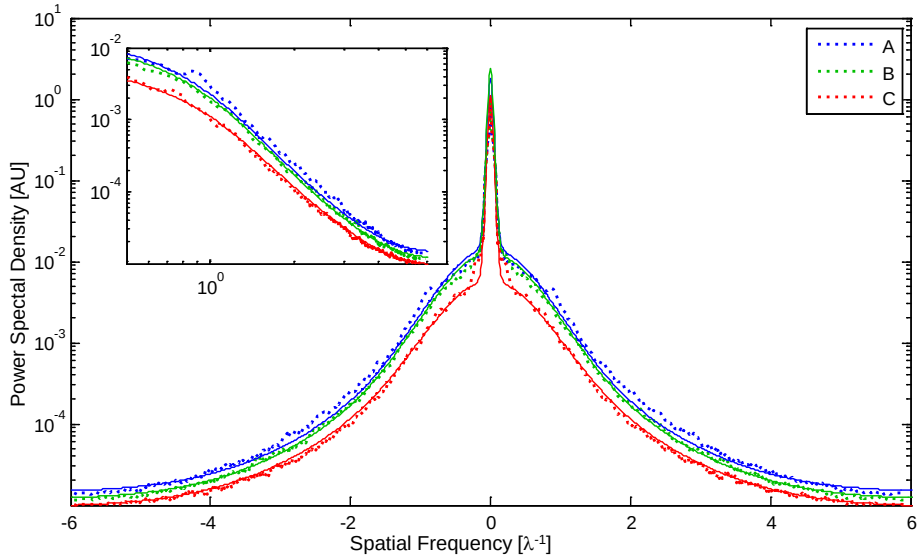

Fig. 3. The power spectral density of CDMP maps calculated for $\delta^P = 4\delta^U$ and different ratios of fields β equal to A) 0.04, B) 0.19, and C) 0.45. Also shown with solid lines are the best fits with power spectrum dependence given in Eq. (9). The inset shows a log-log plot of the high spatial frequencies region.

A different example is illustrated in Figure 10. Here the correlation length of P is kept fixed and is four times larger than the field correlation length but the relative strength β is varied. This corresponds to a gradual progression of different polarization regimes. Again, the most interesting features lie in the high spatial frequencies. When fitting the results of the simulation, only the magnitudes of the Gaussians are altered since now the underlying field correlations of the different components are unchanged. As a result, the PSD are almost parallel to each other in the high spatial frequency range, as can be clearly seen in the inset. One can also note that, at low β, the influence of the correlation length of field P is minimal. This is because, when the average strength of the uniformly polarized component increases, the overall content of high spatial frequencies decreases due to a decrease in the magnitude of the second term in Eq. (9). The values of this magnitude are 3.1, 3.0, and 2.6 for the PSDs labeled A, B, and C, respectively. The behavior seen in Fig. 3 demonstrates that, if the correlations of the underlying fields do not vary during the transition from polarized to globally unpolarized regimes, the shape of the PSD remains relatively unchanged.

There are practical situations when the emerging random electromagnetic fields can be thought as a combination of two interfering mutually coherent fields. When one of these two underlying fields is globally unpolarized and the other one is polarized uniformly, the spatial correlation of the polarization states contains information about both the relative strength and the extent of the field correlations in the two components. The physical situation discussed is typical for random

fields emerging from the interaction between coherent optical fields and randomly inhomogeneous media where a definite polarized component can be associated with ballistic, surface, or single scattering. Our results should be of interest for a variety of applications operating in these scattering regimes.

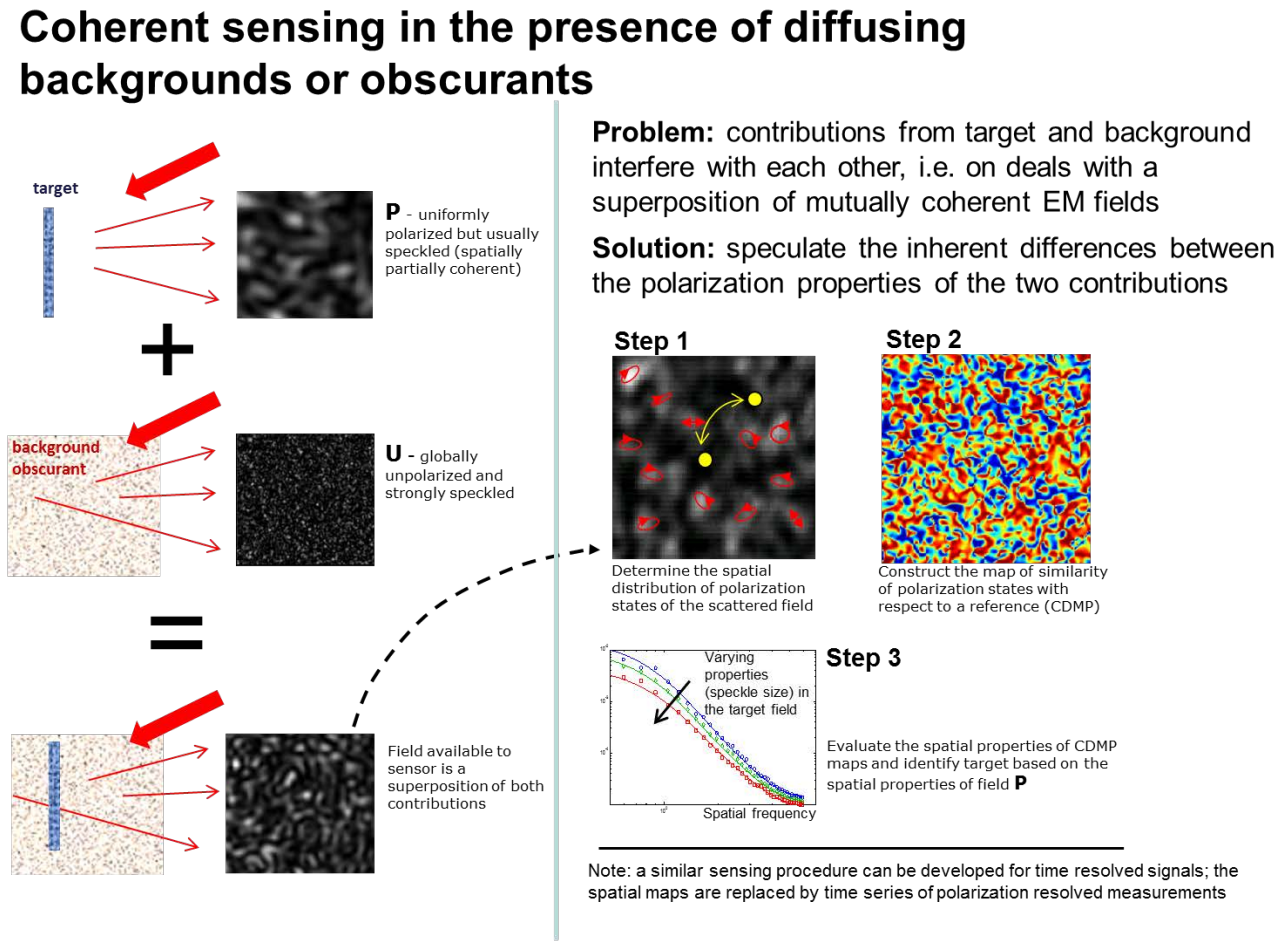

A6 Multi-modal non-imaging active sensing

Active sensing often results on coherent superposition of fields originating from different sources. For instance, a target surrounded by a scattering background will produce a complex "speckle" field in which the useful information is often convoluted with the random contributions from the background. The most challenging situation occurs when the reflection from the target is rather weak compared to this background.

However, because the target material properties are different they impose a unique finger print on the randomly polarized speckle that constitutes the return data. For instance, the target may produce less depolarized reflections. Based on the two-dimensional description of the polarization properties, this information can be extracted.

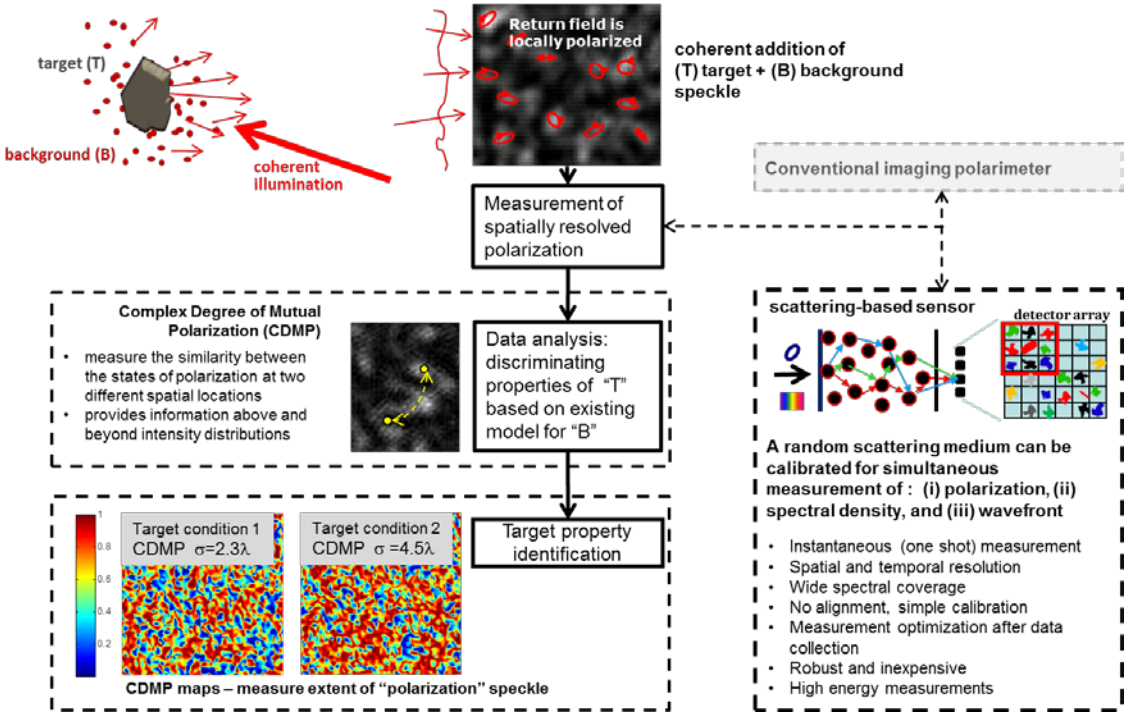

The descriptor of choice is a measure of the similarity between polarization in two different points. Because the target has a unique polarimetric signature, this descriptor allows separating the randomly polarized influence of the background. A model based discrimination can be used to differentiate between different target conditions such as, for instance, different surface roughness or different covering layers on top of diffusing bulk material. We have demonstrated this on laboratory models.

A critical element for this sensing procedure is the possibility to record fast and efficiently a distribution of states of polarization. This can be performed using a conventional imaging polarimeter. However, these instruments have several typical limitations such as their response time, the sensitivity to the input polarization state, and others. Some of the these limitations can be alleviated using a new measurement concept: scattering by a random system constitutes an efficient sampling of incident radiation. Therefore, an appropriate calibration of the scattering process allows using the same "*scattering instrument*" to measure different properties of the incident radiation: spectral, polarization, spatial.

All the measurement procedures rely on measuring scattered intensities. Therefore, the operator can choose to determine, for instance, the spectral composition or the polarization of an input after the actual measurement was actually performed. Moreover, because scattering produces a massive sampling of the input, the measurement can be considerably optimized after the data collection (there are so many independent data samples that one can easily select the most appropriate ones for the task).

In addition, the scattering system can be implemented in conjuncture with typical detector arrays, it is robust, inexpensive and does not require additional alignment once the straightforward calibration is performed.

A7 Backscattering from media with different optical densities

REFs can have different physical origins. REFs that result from scattering of coherent light are fully polarized locally but their global properties can vary from being fully polarized (same polarization state across the entire field) to being completely unpolarized (a uniform distribution of all possible polarization states). For instance, a strong multiply scattering medium will generate fields that are globally unpolarized while a single scattering process will result in a rather uniformly polarized random field. Of course, in addition to different polarization properties, these fields can also differ in their spatial coherence properties, and this diversity may be used to trace their actual physical origin. The present paper provides means to determine the correlation length of such single scattering components in the presence of multiple scattering.

Let us now examine the superposition of two locally polarized fields one being globally unpolarized, $\mathcal{U}(r) = E^{\mathcal{U}}(r)\hat{e}(r)$, and the other one characterized by a uniform polarization state $\mathcal{P}(r) = E^{\mathcal{P}}(r)\hat{e}_0$. If the fields are quasi-monochromatic and mutually coherent, their addition leads to a new REF $E^{\mathcal{R}}(r) = E^{\mathcal{U}}(r)\hat{e}(r) + E^{\mathcal{P}}(r)\hat{e}_0$ with varying global degree of polarization, in a manner similar to combining an unpolarized beam with a fully polarized one to create a partially polarized beam.

The globally unpolarized field U can be modeled as a REF where the complex amplitude components E_x and E_y are both circular gaussian random functions. Each of these components can be represented as a sum of plane waves $E_{\mu}^{\mathcal{U}}(\mathbf{r}) = \sum_j a_j \exp[i(k_j \cdot \mathbf{r} + \phi_{\mu,j})],\ \mu = x, y$, where a_j are the amplitudes, k_j are transverse wavenumbers, $\mathbf{r}$ is a position vector, and $\phi_{\mu,j}$ are uniformly random phases. When $E^{\mathcal{U}}(r)$ is added to a field uniformly polarized along *x*, $E_x^{\mathcal{P}}(\mathbf{r}) = \sum_j b_j \exp[i(k_j \cdot \mathbf{r} + \phi_{x,j})]$, where b_j is a different set of amplitudes, there are several ways to characterize the resultant properties. One simple global measure is to compare the average intensity of the field P with the the average intensity in the total field $E^R(r)$. We note that the ratio $\beta = \left\langle \left| E^{\mathcal{P}}(r) \right|^2 \right\rangle / \left\langle \left| E^{\mathcal{R}}(r) \right|^2 \right\rangle$ of intensities relates to the global degree of polarization, $\bar{P}$, an ensemble quantity specific to the final REF.

Another characteristic of the resultant field is the extent of its field-field correlations. In addition to having different overall magnitudes and polarization characteristics, random fields may also have different field correlation lengths. In other words, the speckle sizes of the fields U and P can be different. The short-range correlation function of U ($\delta^{\mathcal{U}}$) is the same for both *x* and *y* components and is described by $C(\delta^{\mathcal{U}}) = \left\langle E^{\mathcal{U}}(\mathbf{r}) E^{\mathcal{U}}(\mathbf{r} + \delta) \right\rangle$. The unpolarized field can be caused in

different ways. For the purpose of this paper, however, it is assumed that the unpolarized field is examined near the surface of strongly scattering medium and, therefore, its correlation length is of the order of a wavelength.

The field correlation $C(\delta^{\mathcal{P}}) = \left\langle E_x^{\mathcal{P}}(\mathbf{r}) E_x^{\mathcal{P}}(\mathbf{r}+\delta) \right\rangle$ for the linearly polarized component is, of course, only along *x*. In general, a linearly polarized field can result from ballistic propagation as well as from scattering that conserves the state of polarization . Along with the value of β, these two correlation lengths directly influence the length scales of the resulting REF. As mentioned before, β, $\bar{P}$, and the correlation functions C are all global properties, evaluated as ensemble averages. While $\bar{P}$ is indicative of the overlap between the fields U and P, its value does not depend on the spatial correlations characterizing the resulting REF. The correlation function C however, is a structural characteristic evaluated using a two-point property. As the resulting REF has different levels of partial polarization depending on the strength of P, the polarization structure of the final REF is important to consider.

Numerically, REFs with different properties can be overlapped to create different types of Gaussian speckle fields [8]. The coherent superposition of a fully polarized (P) and a globally unpolarized (U) REFs leads to fields with varying degrees of global polarization and different sizes of polarization speckle ($\sqrt{M_2}$ of CDMP maps). This is illustrated in Fig. 11 for different values of the correlation length of P. As can be seen, an increase in $\bar{P}$ corresponds to higher values of $\sqrt{M_2}$, i.e. a larger spatial extent of the CDMP speckle. The global degree of polarization relates the amplitude ratio of the two field component and is experimentally measureable. We also note larger values of $\sqrt{M_2}$ when increasing the correlation length $\delta^{\mathcal{P}}$ of the polarized field. As $\bar{P}$ approaches unity, the uniformly polarized field dominates; thus, the dependence of $\sqrt{M_2}$ on the degree of polarization is stronger in the case of largest correlation length $4\delta^{u}$. It is important to note that as $\bar{P}$ increases, the overall average CDMP also increases which ultimately would result in a uniform, unstructured CDMP map. The addition of the depolarized component leads to the CDMP map structuring.

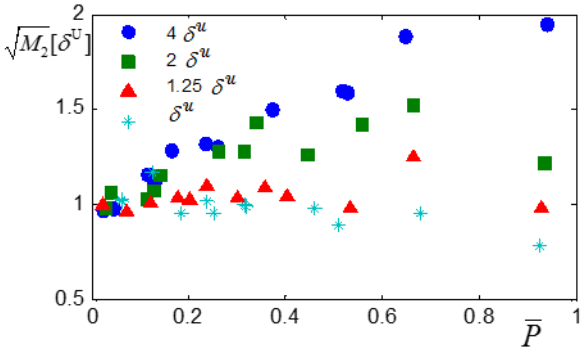

Fig. 15. Values of $\sqrt{M_2}$ of CDMP map correlations as a function of the global degree of polarization $\bar{P}$ for different values of correlation lengths $\delta^{\mathcal{P}}$ as indicated. The correlation length of the globally unpolarized component is δ^{u}.

A proof of concept experiment was designed using a series of colloidal suspensions of different particle sizes and at varying concentrations. In a simplified description, a dense colloidal suspension can be regarded as generating an unpolarized field corresponding to bulk scattering that is overlapped with a uniformly polarized field corresponding to the single scattering component, originating primarily in the vicinity of the medium's boundary as shown in the inset of Fig. 2. In common situations, the contributions from these two scattering components are mixed to produce a partially polarized REF. Increasing the concentration of a colloidal suspension affects its diffusive properties and reduces the transport mean free path l^* of light interacting with it, effectively demonstrating a gradual transition from single to multiple scattering regimes.

The samples were prepared by suspending polystyrene spheres in a Laponite® gel to fix the spheres such that the scattering medium is essentially static. Spheres with diameters of 0.33μm, and 0.43μm were used in different concentrations to create two series of samples having similar values of l^* (3000μm, 2000μm, 1000μm, 500μm, 250μm, and 50μm), as calculated using the appropriate Mie scattering cross-sections and the controlled number density of spheres.

The samples were placed in an imaging setup with NA=0.45 and were illuminated with a 488nm argon laser in a backscattering configuration. The surface of the sample is imaged onto a CCD insuring fully resolved speckles after passing through a Fourier Stokes analyzer. The setup practically records a "close-up" of the REF at the surface of the sample. The corresponding CDMP polarization maps were then calculated from the Stokes images using the polarization state of the incident beam as reference.

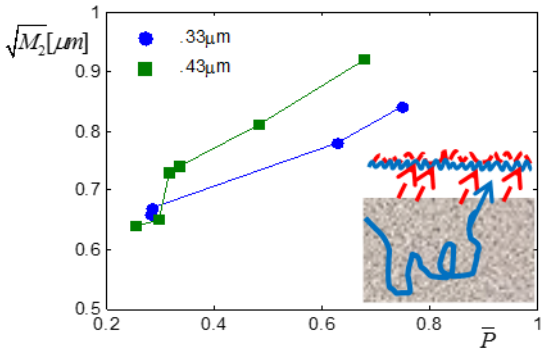

Fig. 16. Experimental dependence of the widths $\sqrt{M_2}$ of CDMP maps correlations as a function of global degree of polarization for media consisting of different particle sizes as indicated. Inset illustrates the different origins of coherently overlapping REFs.

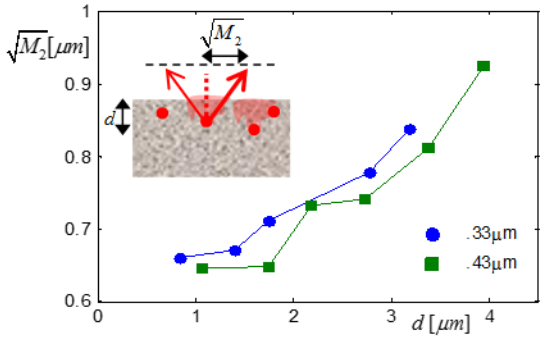

Fig. 17. Experimental plot of the half-width $\sqrt{M_2}$ as a function of average separation d for different particle sizes. Inset illustrates the scattering angle as it relates to $\sqrt{M_2}$ and d.

The second moments corresponding to the autocorrelations of such CDMP maps are plotted in Fig. 12. As can be seen, this relationship between pair-point and point-like properties of the REF follows the general trend observed in the numeric simulations. The value of the second moment rises monotonically with $\bar{P}$, indicating that the size of the polarization speckle increases. Most importantly however is the fact that the rate of this increase depends on the particle size. This happens because of the differences in the corresponding correlation lengths of the uniformly polarized fields P, which represents the polarization maintaining, single scattering component that is specific to each particle size. This difference is clearly observed in Fig. 12 as the dependence on the spatial extent of the P field for the 0.43μm has a steeper slope. The CDMP maps effectively enhance the signature of Mie scattering from particles close to the surface (P) while diminishing the influence of contributions (U) from bulk scattering. Since we measure the properties of REF at the surface, it is expected that $\sqrt{M_2}$ should depend on both the properties of a typical scatter and its average location with respect to the interface as illustrated in the inset of Fig. 13.

Indeed, as evident from Fig. 13, the spatial extent of CDMP speckles depends not only on the average separation *d* between particles as determined by the concentration, but also on the scattering phase function which is specific to particle size. We can use this average separation as a simple estimate for the average distance from a particle to the imaged plane as shown in the inset. A more rigorous analysis of this particle to surface separation may include specific surface properties and the medium's preparation procedures, but this is beyond the scope of the present letter. As the inset suggests, the angular spread of the backscattered field corresponding to a single event can be estimated simply as $\theta = \tan^{-1}\left(\sqrt{M_2}/d\right)$. This value depends only on the scattering phase function and the volume fraction of scatterers and can, therefore, be used to measure the size of the scattering particles. We evaluated the Mie phase functions for the particular sizes of particles used and then integrated them over the angular range corresponding to our system's numerical aperture centered at the backward scattering direction. The phase function was also modified to take into account that the detected intensity depends on the angle at which light is incident onto the detector. Also, light scattered from the small particles decays with distance. Thus, light travelling at different angles traverses different distances untill it reaches the detector. These factors result in an additional weighting coefficient $\cos^3(\theta)$ applied to the phase function. Following this procedure we obtained values of 15.0 and 13.7 degrees for the angular spread of the backscattered field corresponding to particle sizes of 0.33μm and 0.43μm,

respectively. These angles agree quite well with the average scattering angle values of 15.2 and 13.3 degrees obtained experimentally for the corresponding values of distances *d* as determined by the average particle separations.

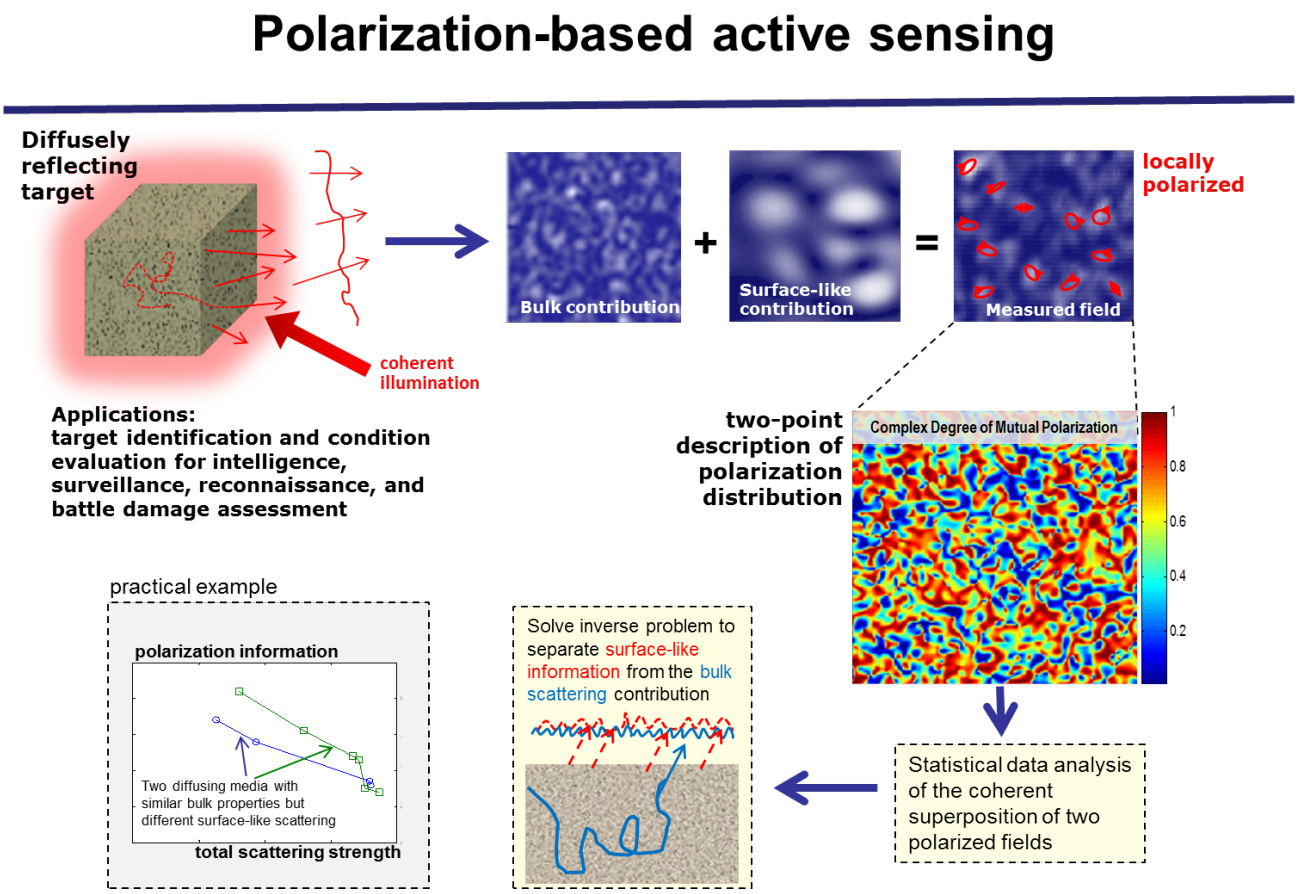

Examining the spatial extent of the CDMP correlation provides a straight measure of the spatial coherence properties of the REF primarily caused by single scattering, which, in turn, is directly related to particle size. Finally, it should be emphasized again that all the information recovered is the result of one single realization of the random interaction between light and matter**.** The demonstrated approach can be extended to many other practical situations of remote sensing where emerging random electromagnetic fields can be thought as a combination of two interfering mutually coherent fields. When one of these underlying fields is globally unpolarized and the other one is polarized uniformly, the spatial correlation of the polarization states contains information about both the relative strength and the extent of the field correlations in the two components.

B. Fluctuation Polarimetry

One of the simplest optical measurements to make is the measurement of the average intensity on a detector. The intensity contains quite a bit of information; it can tell an objects' reflectivity or extinction, for example. If the object is self-luminous, it can reveal the concentration of emitters. Of course, if the intensity is measured in more detail, by using spectral or polarimetric filters for instance, then more can be learned about the origins of the light. For many dynamic systems, it is critical to record higher order moments of the intensity fluctuations rather than just the average. Recently, it was also recognized that information about the shape of the scatterers could be obtained by correlating the intensity fluctuations in different polarization channels to essentially measure the degree of polarization (DOP) of the scattered light in both Gaussian and non-Gaussian scattering regimes.

It is anticipated that more specific and accurate information about the scattering polarizability (particle shape and orientation) could be gained from measuring the state of polarization (SOP) as well. Consider a fluctuating, partially polarized E-field. Let the directions of the major and minor axes of the polarization ellipse be x and y, respectively, and note that this coordinate system is not necessarily aligned with the laboratory frame. Denoting the polarized and unpolarized components of the field with *P* and *U*, respectively, the field at a point r may be written as

$$\mathbf{F}(t) = \left[\left(P_x(t)\exp(i\phi_x(t)) + U_x(t)\exp(i\varphi_x(t))\right)\hat{x} + \left(P_y(t)\exp(i\phi_y(t)) + U_y(t)\exp(i\varphi_y(t))\right)\hat{y}\right]\exp(i\bar{\omega}t),$$

where $\phi_y(t) = \phi_x(t) \pm \pi/2$, depending on the handedness of the SoP. In Eq. (1), *P* and *U* are random variables which in many cases are Rayleigh distributed and φ are random, uncorrelated phases. P_y is fully correlated with P_x since the SoP is not changing in time. The mean frequency of oscillation of the electric field is $\bar{\omega}$. Equation (1) can be regarded as the coherent superposition of four "speckle" fields with their amplitudes and phases fluctuating in both space and time. However, the phase of a given speckle is approximately constant when its amplitude is non-zero. The time of constant phase is referred to as the speckle lifetime.

The relative strengths of the *P* and *U* determine the intensity statistics of the combined speckle pattern. Usually, the *P*' and *U*' components are considered to be slowly varying envelopes relative to $1/\bar{\omega}$, such that one can measure the "short-time" average, $\tilde{I}$, that removes the oscillation at $\bar{\omega}$ but not the fluctuations of the envelope. This is very often, and somewhat misleadingly, referred to as the "instantaneous" intensity, a convention that we will, however, follow for the rest of this Letter. We will omit the tilde from all subsequent intensities.

For E-fields whose components are Gaussian random variables, the second moment of the intensity fluctuations at a point r is $\left\langle(\Delta I(\mathbf{r},t))^2\right\rangle = (1+D^2)\left\langle I(\mathbf{r},t)\right\rangle^2/2$, where *D* is the degree of polarization, $\left\langle I(\mathbf{r},t)\right\rangle$ is the average intensity of the light at the point r, $\Delta I(\mathbf{r},t) = I(\mathbf{r},t) - \left\langle I(\mathbf{r},t)\right\rangle$, and $\langle\ \rangle$ denotes "long-time" averaging. This relationship means that the contrast of the intensity fluctuations (i.e. the second moment normalized to the mean) is in fact given by the amount of correlation between the orthogonal E-field components, i.e., the degree of polarization. This is analogous to determining *D* by measuring the fluctuations in two, orthogonally polarized channels at the same time, as is frequently done, and calculating the cross-correlation between the measurements.

Unfortunately, SOP cannot be inferred from the fluctuations of the instantaneous intensity. This is simply because the SOP depends on the phase Δ between the polarized E-field components and its measurement which would require a time resolution better than $1/\bar{\omega}$. We can, however, go further if we bring in a reference field, R. We will choose the reference to have a non-fluctuating intensity with the same mean frequency as F. For simplicity, this will be a linearly polarized field whose orientation can be controlled at will. Most importantly, because of the random nature of the

phases in Eq. (1), this reference can be incoherent with respect to the fluctuating field, meaning that no stable interference is observed when R and F, or any component of F, are superposed. Nevertheless, during the speckle lifetime, the two fields can interfere. If the fluctuating field is fully polarized along the same direction as the reference, the resulting intensity statistics follow a Rician distribution. In general, the statistics are more complicated because the intensity fluctuations arising from the polarized components of the field will be partially correlated based on the SOP of the fluctuating field. However, as we will show below, the full polarimetric description of the field F can be recovered by measuring the intensity statistics of the superposition as the polarization orientation of the reference field changes.

If the intensity of the linearly polarized reference field is $|\mathbf{R}|^2$, the instantaneous intensities along the major and minor axes of the polarization ellipse of F are $|R_x(\theta)|^2 = |\mathbf{R}|^2 \cos^2(\theta), |R_y(\theta)|^2 = |\mathbf{R}|^2 \sin^2(\theta)$, where θ is an unknown angle between the reference field orientation and the x-axis.

The instantaneous intensity of the fluctuating field can be decomposed into four parts: a polarized and an unpolarized intensity along both x and y axis. These following relations will hold for the intensities: $D\langle|\mathbf{F}|^2\rangle = \langle P_x^2\rangle + \langle P_y^2\rangle$, $(1-D)\langle|\mathbf{F}|^2\rangle = \langle U_x^2\rangle + \langle U_y^2\rangle$, $P_y^2 / P_x^2 = A$, $0 \le A \le 1$ $\langle U_y^2\rangle / \langle U_x^2\rangle = 1$. The first two equations simply mean that the (un)polarized component of the intensity is the sum of the (un)polarized intensities along the axes of the polarization ellipse. The third relation defines the square of the ellipticity, which is constant during the measurement. Upon long-time averaging, the unpolarized intensities are equally divided between the two axes as expressed in the last relation. Note that the ratio of the instantaneous unpolarized intensities is unbounded because they fluctuate in an uncorrelated manner .

When superposing the fields R and F, the instantaneous intensity can be expressed as $I(\theta) = \sum_i I_i(\theta), i = x, y$ where

$I_i(\theta) = P_i^2 + R_i^2(\theta) + U_i^2 + 2P_iR_i(\theta)\cos(\phi_i) + 2P_iU_i\cos(\phi_i - \varphi_i) + 2U_iR_i(\theta)\cos(\varphi_i)$.

Since the phases are random, we see that the first moment of the intensity fluctuations is simply $\langle I(\theta)\rangle = \langle|\mathbf{F}|^2\rangle + \langle|\mathbf{R}|^2\rangle$. To calculate the second moment, we recall that the magnitudes of the components of the fluctuating field are Rayleigh random variables and, therefore, the intensities are exponential random variables and so $\langle I^2\rangle = 2\langle I\rangle^2$. The second moment of $I(\theta)$ can be found to be

$$\left\langle \left(I(\theta) - \langle I(\theta)\rangle\right)^2 \right\rangle = \left[(1+D^2)/2\right]\left\langle|\mathbf{F}|^2\right\rangle^2 + \left\{2D\left[1+(A-1)\sin^2(\theta)\right](1+A)^{-1} + (1-D)\right\}\left\langle|\mathbf{F}|^2\right\rangle\left\langle|\mathbf{R}|^2\right\rangle.$$

Finally, using the calculated moments one can evaluate the contrast of the intensity fluctuations as $C = \sqrt{\left\langle \left(I(\theta) - \langle I(\theta)\rangle\right)^2 \right\rangle} / \langle I(\theta)\rangle$. This shows that the intensity fluctuations of the superposition depend on D, A, and θ, which provide all of the single point polarimetric information, up to the handedness of the polarization ellipse.

The second term highlights the interferometric nature of the measurement at short time scales; it is the "interferometric gain" that comes from mixing the reference and fluctuating fields. While C decays as $|\mathbf{R}|^{-1}$ for $|\mathbf{R}| >> |\mathbf{F}|$, the actual magnitude of the intensity fluctuations increases as $|\mathbf{R}|$. The ability to controllably enhance the strength of the intensity fluctuations may prove very useful for measurements of weak fields.

The development was tested experimentally on a fluctuating field created using two rotating diffusers illuminated by a laser beam. A polarizer and quarter waveplate were placed after one of the diffusers to create a fully polarized fluctuating field. The other diffuser created the unpolarized

part that was added to the polarized component in order to control D. The reference field was obtained by diverting a small part of the initial beam before the diffusers, and the total fluctuating intensity, i.e. the intensity of the overlapped polarized, unpolarized, and reference fields) was measured using a photodiode. The contrasts calculated from the measured intensity fluctuations (dots) and from theory are shown in Fig. 14 for different fluctuating fields. The lines were obtained by finding the D, A, and initial θ that minimized the RMS difference between the experimental and theoretical contrasts; the fitting procedure will be discussed in more detail later.

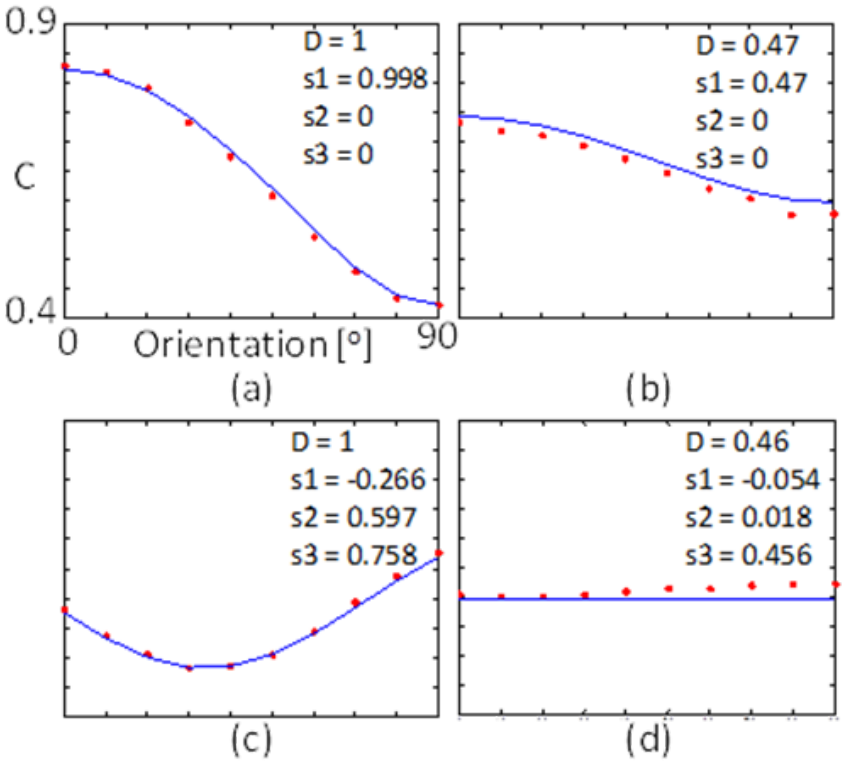

Fig. 84 The experimental (red dots) and theoretical (blue line) intensity contrasts for (a) vertically polarized, (b) partially vertically polarized with $D \approx 0.455$, (c) elliptically polarized, and (d) unpolarized fluctuating fields as a function of the orientation of a linearly polarized reference field. All of the plots are on the same scale. The DoP and Stokes vector for the best fit to the experimental contrasts are shown on each plot.

Figure 14 clearly indicates a strong dependence of the contrast on the SOP of the fluctuating field, rather than just its DOP. Each of the experimental contrasts in Fig. 14 was calculated by recording approximately 500 intensity speckles. The variation of the contrasts from repeating the experiment (i.e. different realizations of the 500 speckles) in the same configuration is smaller than the symbols in the figure. The measured intensity fluctuations are related directly to the DOP; a field with stronger normalized fluctuations has a correspondingly higher DOP. In our experiment, the DOP of the measured field is not constant; we alter the DOP of the measured field by changing the orientation of the linearly polarized reference field. For example, if the fluctuating field is linearly polarized, then the total field is fully polarized when the reference field is aligned with the fluctuating field even though the two fields are incoherent with one another. As the orientation of

the reference field is changed, however, the DOP of the total field, and thus the resulting intensity fluctuations, decreases.

Finally, we note that in order to determine an unknown Stokes vector from the values of the measured contrasts requires the use of numerical techniques because, while closed-form solutions for the variables in Eq. (7) exist, the equations are transcendental. Fortunately, the solution domain is finite with $A \in [0,1], \theta \in [0,\pi)$, and $D \in [0,1]$. In principle, D can be determined by simply measuring the intensity fluctuations with the reference field off and then applying Eq. (2), thus reducing the dimensionality of the solution domain. As noted earlier, the solid lines in Fig. 14 were obtained by fitting the model to the contrasts calculated from the experimental data. To perform the fit, the *A* and *D* axes were divided into 101 evenly spaced increments from 0 to 1, and the θ axis was divided into 180 evenly spaced increments from 0 to 179º. For each possible configuration the RMS difference between the experimental contrasts and the theoretical contrasts was calculated. The set of [*A*, *D*, θ] with the smallest RMS difference was selected as the estimated DOP and SOP.

The Stokes vector may be defined in terms of [*A*, *D*, θ] as

$\chi = \tan^{-1}(\sqrt{A}), \quad s_1 = D\cos(2\theta)\cos(2\chi), s_2 = D\sin(2\theta)\cos(2\chi), s_3 = D\sin(2\chi)$ where χ is the ellipticity angle. The calculated Stokes parameters are only interesting if they are unique to a particular set of contrast measurements. The uniqueness of the results can be determined by noting that the right had side of the equation has the form $G(A,D) + H(A,D)\sin^2(\theta)$ where G and H are constants that are determined by A and D. If there are there is another combination of A and D which we will call (A',D') such that $G(A,D) = G(A',D')$, and $H(A,D) = H(A',D')$, then an identical $C(\theta)$ would be obtained for multiple polarization states. However, those two equalities are only non-trivially satisfied by $A' = 1/A$ and $D' = -D$, both of which are non-physical. As a result, we can concluded that $C(\theta)$ is in fact uniquely determined by A and D, and that finding the A and D that produce the best fit to the measured data will yield the correct SoP.

This new method extracts the state of polarization of a fluctuating field from the first two moments of the distribution of intensity fluctuations. The key is to mix the fluctuating field with an uncorrelated reference. The short term interferences between these fields influence the intensity fluctuations in a manner that depends on the state of polarization of the fluctuating field. Analyzing the residual state of polarization of optical fields is of interest for a number of sensing applications that rely on light scattering. Most polarimetric techniques require either discarding part of the light of interest due to the use of polarimetric filters or splitting the light among multiple detectors; however, if the intensity fluctuations are being measured, the SoP of the signal can be determined without additional detectors or polarization optics. In addition, because the method is interferometric in nature it may be especially appropriate for measurements of weakly scattering systems.

C. New paradigms for light-matter interaction

Direct mechanical action of radiation is due to momentum transfer. As a result of scattering and/or absorption, the momentum of light is always decreasing along the direction of incidence z and, consequently, a positive momentum is transferred to the object. If $p=hw/c$ is the incident momentum per photon, the most one can transfer to an object is $2p$ or p when the object is completely reflecting or absorbing, respectively. This effect of direct radiation pressure has been considered in the context of perturbing satellite orbits as well as space propulsion. The magnitude of the force per unit area is proportional to the incident intensity.

C1 Nonconservative forces on scattering objects

To understand why nonconservative forces are usually pressure, not drag, forces, let us consider the situation where a plane wave propagating along z direction is scattered by an object. Part of the wave's momentum is transferred to the scattered radiation that is deflected away and, therefore, some of the initial momentum along z-direction is lost even for nonabsorbing objects.

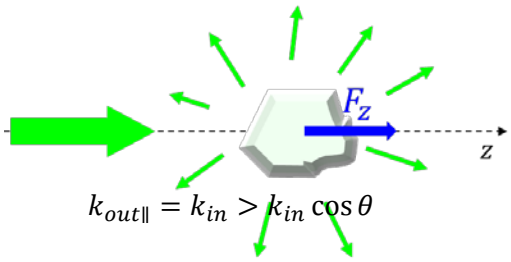

Fig. 15 Conservation of linear momentum in scattering.

Due to momentum conservation, the lack of wave's momentum along z after scattering should be compensated by the momentum transferred to the scattering object. This means that, during any kind of scattering event, the wave imparts a certain amount of momentum to the scattering body creating a force acting in the positive z direction, i.e. along the wave's propagation. This radiation pressure depends on the light intensity I and the objects' reflectivity R as $p = (I/c)(1+R)$ where c is the speed of light. For objects with specific shapes, the redistribution of light momentum can lead to unexpected movements of the object. Depending on the scattering phase function, the radiation pressure can act in a direction different than the incidence, a fact that is also known from the theory of anisotropic scatterers. However, in all these situations, some amount of momentum along the direction of light incidence is lost and this makes it impossible for a scattering object to move in a direction opposite to that of the incident beam. This is depicted schematically in Figure 15.

To increase the "forward" momentum resultant from the scattering or, in other words, to create a negative force on the object, one can use an active medium as suggested in Ref. [9]. However, this approach is only of limited practicality as most objects do not manifest optical gain. Alternatively, instead of artificially adding extra "forward" momentum to the scattered field, one could input from the beginning less momentum along z.

Fig 16. A generic optical device ("black box") converts the incident waves into waves propagating along the z-axis. As a result of momentum conservation, a negative optical force is generated.

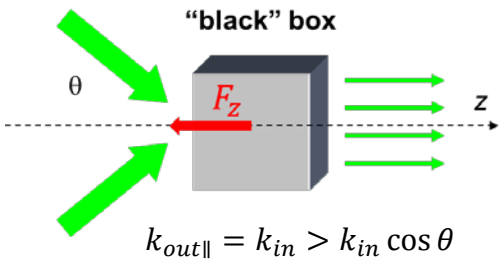

The simplest way to achieve this momentum increase however is by illuminating with waves that propagate at some angle θ with respect to the *z*-axis and have the nonabsorbing scattering object (the "black box" depicted in Fig. 16) redirect these partial waves along the *z*-axis. Assuming that this "black box" does not produce additional scattered waves, the momentum conservation law is simply $k_{wave}\cos\theta = k_{wave} + k_{box}$ and the force acting on the object becomes $F_z = (P/c)(\cos\theta - 1)$, where P is the total optical power incident on the object. It follows that the resultant force on the object is negative for any $\theta \neq 0°$. This somewhat counterintuitive consequence has now been demonstrated in a number of physical arrangements.

C2 Predesigned nonconservative forces - structured beams of light

Configurations generating negative, nonconservative forces can be created by structuring optical beams. We will examine here the practically relevant example of nondiffracting beams that maintain their structure over large distances, but concept is not limited to only these types of beams. A beam manifests nondiffractive behavior when its plane wave decomposition contains only one component of the tangential wavevector. In the paraxial approximation, such beam propagating along *z* can be described as

$$E(\mathbf{r}) = E(x,y)\exp(ik_z z), E(x,y) = \int_{-\pi}^{\pi} A(\varphi)\exp[ik_t(x\cos\varphi + y\sin\varphi)]d\varphi,$$

where the wavenumber k in the surrounding medium is $k^2 = k_t^2 + k_z^2$. Due to the radiation pressure, the time-averaged force exerted on a particle with dimensions much smaller than the wavelength is $\mathbf{F}_{rp} = (k/2)\,\mathrm{Im}\,\alpha\,\mathrm{Re}(\mathbf{E}\times\mathbf{H}^*)$, where α is the particle's polarizability. Further use of the Maxwell's equations leads to the *z*-component of the force: $F_{rp}^z = \frac{1}{2}\mathrm{Im}\,\alpha\,|E(x,y)|^2\,k_z$. Note that, in the paraxial approximation, the radiation pressure is due only to the nonconservative force acting along *z*. It follows that, when the beam is described by one single propagation constant, F_{rp}^z is always positive, i.e. it acts along the propagation of the beam as illustrated in Figure 15.

However, the situation may be different when several nondiffractive beams, each characterized by its own k_z, are coherently superposed. For instance, in the case of a beam with two propagation constants $E(\mathbf{r}) = E_1(x,y)\exp(ik_{1z}z) + E_2(x,y)\exp(ik_{2z}z)$, one can easily check that the extremum of the radiation pressure force is reached if

$\frac{|E_1(x,y)|}{|E_2(x,y)|} = -\frac{(k_{1z}+k_{2z})\cos\gamma}{2k_{1z}}$, where $\gamma = (\phi_1 - \phi_2) + (k_{1z} - k_{2z})z$ and $\phi_i(x,y) = \arg E_i(x,y)$. The z-component of the force reaches its minimum for $\cos\gamma = -1$ when $(F_{rp}^z)_{\min} = -\frac{1}{8}\mathrm{Im}\,\alpha\,|E_2(x,y)|^2\,(k_{1z}-k_{2z})^2/k_{1z} < 0$.

Thus, in this system of interfering nondiffracting beams, there are locations where the Poynting vector is oriented in a direction opposite to the beam propagation and, consequently, the radiation pressure acts towards the source of light!

It is interesting to note that for this kind of beam, the electric field energy density is

$$|E(\mathbf{r})|^2 = |E_1(x,y)|^2 + |E_2(x,y)|^2 + 2|E_1(x,y)||E_2(x,y)|\cos\gamma$$

And, when $|E_{1,2}(x,y)|$ are slowly varying functions of coordinates, because in the vicinity of points where optical force is negative $\cos\gamma = -1$ it means that these points are also local minima of $|E(\mathbf{r})|^2$. It is known that, because of gradient forces, small particles with negative polarizability tend to move towards the regions with lowest electric field density. Examples include low-index particles in a water, metal particles or blue-detuned atoms. Nevertheless, points where the radiation force points against the average flow of energy can be found in local maxima of intensity for appropriate construct of field $|E_{1,2}(x,y)|$.

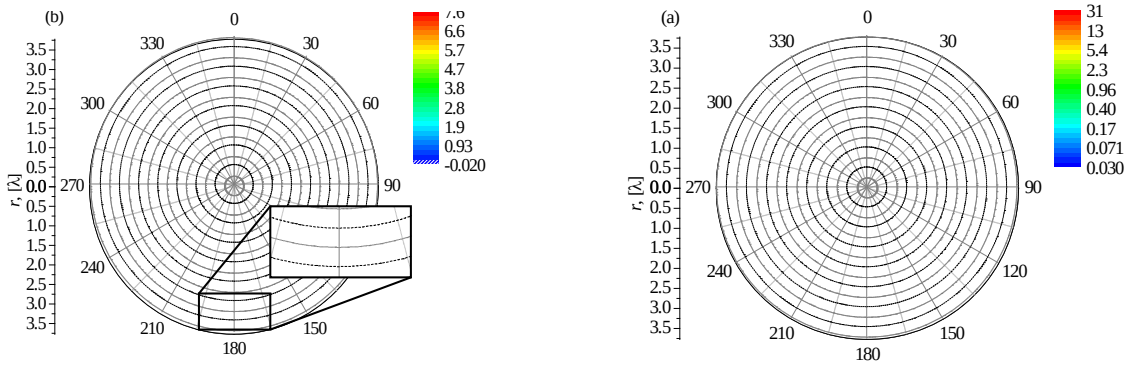

Fig. 17 Distribution of electric energy density (a) and optical force in arbitrary units (b). The calculations correspond to the case of a silver nano-particle suspended in carbon tetrachloride with refractive index 1.46. The shaded area at the bottom of figure (b) denotes the NOF region. The inset shows only the nonconservative part of the force.

In Figure 17a, the distribution of electric field density $|\mathbf{E}(r,\varphi)|^2$ is shown in the cross-section of such a beam obtained by interfering a plane wave with a Bessel beam of order -1 and $k_z = 0.8k$. Figure 17b illustrates the distribution of *z*-component of the force acting on a small particle when the beams parameters are such that the F_{ng}^z reaches its minimum near the point of coordinates $r \approx 3.14\lambda$ and $\phi \approx \pi$, which correspond to the minimum of $|\mathbf{E}(r,\varphi)|^2$ in Fig. 3a.

The region where the force is negative extends along the entire propagation distance for such non-diffracting, rotating, scale-invariant vector electromagnetic waves. Our estimations show that the dimensions of such regions and the magnitude of the forces can be further controlled by interfering a larger number of beams, by considering beams with more complex angular spectra or by using other transformations between different propagation planes.

C3 Adaptive nonconservative forces on scattering objects

Scattering objects may have irregular shapes or inhomogeneous distribution of their optical properties. In this situation, the scattering is a rather complicated process that depends on scatterer morphology, orientation, as well as the properties of incident radiation. We have recently demonstrated that even in such extreme situation one can find the appropriate conditions in which the overall mechanical action can be directed at will.

We will illustrate the extreme situation of a cluster like object that scatters the light such that the original direction of propagation of any incident photon is completely randomized through the scatterer. This object scatters light in all directions and generates an uncorrelated, speckle like field. The complex object is illuminated by an electromagnetic field considered to be the superposition of a number of plane waves whose corresponding phases and polarizations can be adjusted at will. By adjusting these properties one can effectively transform the random medium into a useful optical component, such as, for instance, a focusing lens. In one such adjustment of the incident field, it can be found that all the scattered partial waves interfere constructively along the z-direction, in a manner similar to the one produced by the "black box" suggested in Figure 16. Of course, different plane waves constituting the incident beam contribute differently to the force along z. For instance, a plane wave traveling originally along the z-axis can create only a pushing force ($\theta = 0$) while plane waves incident perpendicularly to the z-axis ($\theta = \pi/2$) contribute the most to the negative force F_z. Obviously, there should be an angle of incidence θ_m at which the plane wave contribution to F_z is zero and observable negative forces can only be achieved for $\theta > \theta_m$.

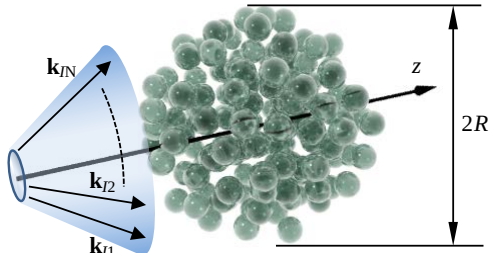

Fig. 18 Complex cluster of spheres illuminated by an adjustable wavefront.

The minimal angle θ_m at which F_z is still negative can now be estimated. Let us assume that the random object scatters light evenly into N_s independent channels corresponding to the number of speckles in the far field. When the incident beam is composed of N_i partial plane waves, the momentum of light scattered along z-direction due to constructive interference of these partial waves is $k_{sz} = (P_s/c)N_i^2/N_s$, where P_s is the scattered power for one particular plane wave. On the other hand, the total initial momentum along z is $k_{iz} = (P_s/c)N_I \cos\theta$. Thus, in order for the electromagnetic momentum to increase due to scattering, the condition $\cos\theta \le N_i/N_s$ should be fulfilled.

We exemplify this concept on a cluster of spheres which is illuminated by a set of coherent plane waves uniformly distributed in the *k*-space such that all have the same k_z component as shown in Figure 4. Note that this condition makes the overall beam nondiffracting. In general, the multiple scattering from such inhomogeneous objects is complicated and not isotropic and the details of the process can only be described numerically. In this case, scattering from the aggregate was calculated using a multiple sphere T-matrix FORTRAN code. For this example, hundreds of spheres with size parameter $kr = 1$ were randomly distributed within a spherical volume with size parameter $kR = 10$ ($R \approx 7l^*$), they were illuminated by a nondiffracting beam and the amplitude scattering matrices were calculated along every scattering direction. The angular distribution of the scattered field in the forward scattering hemisphere is shown in Figure 19a for the case where the plane waves constituting the illuminating beam have all the same phase. The ring of high field amplitude (mostly green) corresponds to the forward scattering direction for each partial plane wave.

Next, we attempted to maximize the scattering along z-axis by adjusting the polarization and phase of each plane wave in such a way that the x-components of all partial scattered fields along z-direction are maximized and in phase. The resulting scattering pattern is shown in Figure 19b

where one can clearly see the spot of enhanced scattering located at zero polar and azimuthal angles, i.e. along the direction of beam's propagation.

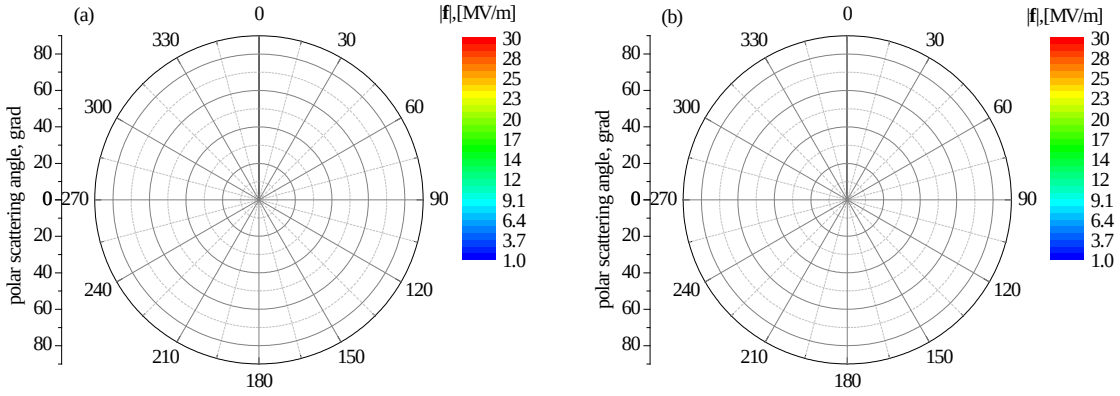

Figure 19. (a) Angular distribution of scattered electric field amplitude $|\mathbf{f}|$ in the forward scattering hemisphere of the cluster shown in Fig. 17. (b) Same for conditions where the illumination is optimized such that forward scattering is maximized.

Having access to the scattering distribution one can evaluate the magnitude of the optical force

$$\mathbf{F}_{opt} = -\frac{\varepsilon_0}{2k^2}\int_{\Omega}\left|\mathbf{f}(\hat{k}_s = \hat{r},\{\hat{k}_{Ii}\})\right|^2 \hat{r}d\Omega + \frac{2\pi\varepsilon_0}{k^2}\sum_{i=1}^{N_I}\hat{k}_{Ii}\,\mathrm{Im}\left[\mathbf{f}(\hat{k}_s = \hat{k}_{Ii},\{\hat{k}_{Ii}\})\cdot\mathbf{E}_{Ii}^*\right],$$

where the scattering amplitude $\mathbf{f}(\hat{k}_s,\{\hat{k}_{Ii}\})$ depending on both on the direction of scattering $\hat{k}_s$ and the directions of propagation of every partial wave $\hat{k}_{Ii}$ describes the scattered field in the far zone $\mathbf{E}_s = (\exp(ikr)/(kr))\mathbf{f}(\hat{k}_s,\{\hat{k}_{Ii}\})$. The numerical estimation of the integral for the situation depicted in Fig 19a results in a value of the force $F_z = 1.5\,\mathrm{pN}$. For optimized conditions of illumination corresponding to Fig 19b, however, the optical force along z-direction becomes negative: $F_z = -0.24\,\mathrm{pN}$.

These results based on this principle of conservation of linear momentum, suggest that nonconservative optical forces acting on any scattering object can be manipulated at will without limitation of their shapes or structural morphology. Notably, in certain circumstances, the overall force acting on the object can point even in a direction opposite to beam's propagation.

The structured illumination concept introduced here can be further improved as we will discuss further in this proposal. More elaborate optimization procedures that not only maximize scattering in the desired direction, but also minimize scattering along other directions can be used to control the angle of convergence for partial plane waves and the entire structure of the beam.

A material system can modify the radiation structure which, in turn, affects the mechanical effects on matter. As an example, we demonstrated the strong coupling between optical radiation and a colloidal system: changing the particles arrangement changes the field configuration acting on them, which influences the movement of the particles and so on. We have demonstrated for the first time that the "dynamic speckle" can be coupled to the "particles dynamics" without any thermal dissipation (absorption) into the system. The phenomenology is common to many complex systems (bio, turbulence, plasmas, etc.), which are in "*steady state*" but not in "*thermodynamic equilibrium*" because energy is continuously given to system's constituents. So far, fundamental understanding was always hindered by the lack of controllable laboratory experiments. This all-optical "*active medium*" may serve as a convenient tool.

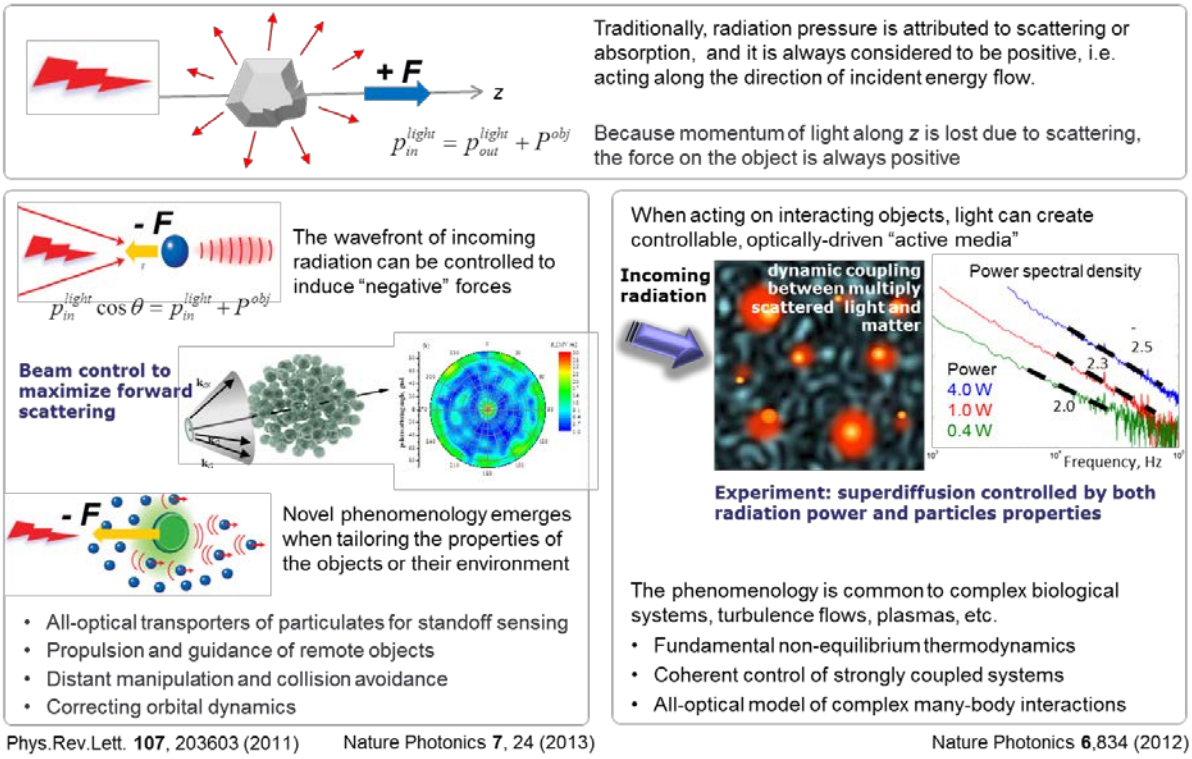

Phys.Rev.Lett. **107**, 203603 (2011) Nature Photonics **7**, 24 (2013) Nature Photonics **6**,834 (2012)

Even though our experiments are small scale demonstrations, the average field strength inside the cavity containing the colloid was only about one order of magnitude higher than that corresponding to solar irradiance (cca 1kW/m^2). It is expected that, in the absence of drag forces (due to the liquid for our colloid), such radiation-mediated binding can occur at even lower field strengths.

Publications during reporting period:

Journals

1. Aristide Dogariu and Remi Carminati, *Electric Field Correlations in Three-Dimensional Speckles,* Physics Reports **559**, 1-29 (2015)
2. J. Broky and A. Dogariu, *Polarization correlations in backscattering from media with different optical densities*, Opt. Lett. **39**, 1465 (2014)
3. S. Sukhov, K. M. Douglass, and A. Dogariu, *"Dipole-dipole interaction in random electromagnetic fields",* Opt. Lett. **38**, 2385 (2013)
4. M. Dubreuil, P. Delrot, I. Leonard, A. Alfalou, C. Brosseau, and A. Dogariu, *Exploring underwater target detection by imaging polarimetry and correlation techniques*, Appl. Opt. **52**, 997 (2013)
5. A. Dogariu, S. Sukhov, and J. J. Sáenz, *The optically-induced "negative forces"*, Nature Photonics **7,** (2013)
6. D. C. Kohlgraf-Owens, S. Sukhov, and A. Dogariu, "*Near-Field Topography of Light*", Optics and Photonics News **23**, 39 (2012)
7. K.M. Douglass, S. Sukhov, and A. Dogariu, *Superdiffusion in optically-controlled active media,* Nature Photonics **6**, 834 (2012)
8. D. C. Kohlgraf-Owens, S. Sukhov, and A. Dogariu, *"Discrimination of Field Components in Optical Probe Microscopy"*, Opt. Lett. **37**, 3606 (2012)
9. T. Kohlgraf-Owens, and A. Dogariu, "*Fluctuation Polarimetry*", Opt. Lett. **37**, 1961 (2012)
10. S. Sukhov, D Haefner, J. Bae, D. Ma, R. D. Carter, A. Dogariu, *The effect of spatial coherence on scattering from optically inhomogeneous media,* JOSA **A29**, 85 (2012)
11. S. Sukhov, V. Kajorndejnukul, D. Haefner, G. Agarwal, and A. Dogariu, *"Surface-induced optical anisotropy of inhomogeneous media",* Photonics and Nanostructures **11**, 213 (2013)
12. S. Sukhov and A. Dogariu, *Negative Nonconservative Forces: Optical "Tractor Beams" for Arbitrary Objects,* Phys. Rev. Lett. **107**, 203602 (2011).
13. J. Broky and A. Dogariu, "*Correlations of polarization in random electro-magnetic fields",* Opt. Express **19**, 15711 (2011)
14. S. Sukhov and A. Dogariu, *"On the concept of "tractor" beams"*, Opt. Lett. **35**, 3847 (2010)
15. J. Broky and A. Dogariu, "Complex degree of mutual polarization in randomly scattered fields", Opt. Express 18, 20105 (2010)
    T. W. Kohlgraf-Owens and A. Dogariu, "Transmission matrices of random media: means for spectral polarimetric measurements", Opt. Lett. 35, 2236 (2010)
16. S. Sukhov, D. Haefner and A. Dogariu, "Stochastic reconstruction of anisotropic polarizabilities", J. Opt. Soc. Am. A **27**, Issue 4, pp. 827-831 (2010)

Conference proceedings and Presentations

1. S. Sukhov, A. Shalin, and A. Dogariu, *Ultra-Fast Motion of Optically Driven Metallic Nanoparticles*, CLEO/QELS, San Jose, June 2014.
2. S. Sukhov, V. Kajorndejnukul, A. Dogariu, *Adaptive nonconservative forces on scattering objects*, Saint Petersburg, Russia, June 2014.
3. J. Broky and A. Dogariu, *Identifying scattering functions from polarization correlations in backscattering*, SPIE Annual Meeting, San Diego, August 2013
4. S. Sukhov, K.M. Douglass, and A. Dogariu, *Pair Interaction and Optical Binding in 3D Random Electromagnetic Fields*, SPIE Annual Meeting, San Diego, August 2013
5. V. Kajorndejnukul, W. Ding, S. Sukhov, CW Qiu, A. Dogariu, *Negative Optical Forces at Dielectric Interfaces for Long Range Particle Manipulation*, SPIE Annual Meeting, San Diego, August 2013
6. K.M. Douglass, S. Sukhov, and A. Dogariu, *Forces in Random Electromagnetic Fields*, CLEO/QELS, San Jose, June 2013.
7. V. Kajorndejnukul, W. Ding, S. Sukhov, C.-W. Qiu, A. Dogariu, *Experimental Demonstration of Negative Optical Forces at Dielectric Interfaces*, CLEO/QELS, San Jose, June 2013.
8. V.Kajorndejnukul, S. Sukhov, D. Haefner, G. Agarwal, and A. Dogariu, *Surface Induced Anisotropy and its Optical Manifestation: Anomalous Spin Hall Effect*, FIO, Rochester (2012)
9. K. M. Douglass, S. Sukhov, and A. Dogariu, *optically-controlled active media*, FIO, Rochester (2012)
10. Sergey Sukhov, David Haefner, Aristide Dogariu, *Conservation of Angular Momentum and Nonconservative Optical Forces in Scattering*, PIERS, Moscow, (2012)
11. Sergey Sukhov, Veerachart Kajorndejnukul, David Haefner, Aristide Dogariu, Surface *Induced Refractive Index Variations in Inhomogeneous Slabs*, PIERS, Moscow, (2012)
12. Thomas Kohlraf-Owens and A. Dogariu, *Intensity Flutuation Polarimetry*, Hyperspectral/Polarimetric Community Collaboration Workshop, Huntsville , AL (2012)
13. Thomas Kohlraf-Owens and A. Dogariu, *High-order Polarimetry for Target Identification*, Hyperspectral/Polarimetric Community Collaboration Workshop, Huntsville, AL (2012)

14. Dana Kohlgraf-Owens, Sergey Sukhov, and Aristide Dogariu, *Exploiting Optical Forces to Characterize Electromagnetic Fields*, FIO/OSA annual meeting, San Jose (2011)

15. John Broky and Aristide Dogariu, *Correlations of polarization in random electromagnetic fields*, FIO/OSA annual meeting, San Jose (2011)

16. Sergey Sukhov*, David Haefner, Janghwan Bae, Deqiang Ma, R. Douglas Carter, and A. Dogariu, *Scattering of Partially Coherent Radiation from Optically inhomogeneous Medi*, FIO/OSA annual meeting, San Jose (2011)

17. Thomas Kohlgraf-Owens and Aristide Dogariu, *Imaging Spectroscopy Without a Spectrometer*, FIO/OSA annual meeting, San Jose (2011)

18. Thomas Kohlgraf-Owens and Aristide Dogariu, *Intensity Fluctuation Polarimetry*, FIO/OSA annual meeting, San Jose (2011)

19. S. Sukhov and A. Dogariu, *Optical "tractor beams" with nonconservative forces, CLEO/IQEC, Baltimore, (2011)*

20. S. Sukhov, D. Haefner, A. Dogariu, D. Ma, D. Carter, *Stochastic Scattering Approach to Determine Effective Packing Structure in Diffuse Optical Coatings*, TAPPI, Munich Oct 2010

21. David Haefner, Sergey Sukhov, Aristide Dogariu, *Nonconservative Optical Torques*, CLEO/IQEC, San Jose, (2010)

22. K. M. Douglass, T. Suezaki, S. John, andA. Dogariu, *Reflection of Subdiffusive Light from 3D Disordered Photonic Crystals*, CLEO/IQEC, San Jose, (2010)

23. Kyle M. Douglass, Gabriel Biener, Sergey Sukhov, Aristide Dogariu, *Rotational Stochastic Resonance*, CLEO/IQEC, San Jose, (2010)

1.

1. Report Type

Final Report

Primary Contact E-mail
Contact email if there is a problem with the report.

apotter@ucf.edu

Primary Contact Phone Number
Contact phone number if there is a problem with the report

407-882-2018

Organization / Institution name

University of Central Florida

Grant/Contract Title
The full title of the funded effort.

Sensing Random Electromagnetic Fields and Applications

Grant/Contract Number
AFOSR assigned control number. It must begin with "FA9550" or "F49620" or "FA2386".

FA9550-10-1-0190

Principal Investigator Name
The full name of the principal investigator on the grant or contract.

Aristide Dogariu

Program Manager
The AFOSR Program Manager currently assigned to the award

Dr. Julie Moses

Reporting Period Start Date

05/01/2010

Reporting Period End Date

04/30/2010

Abstract

Random electromagnetic fields (REF) exist in all forms and one common origin is a result of the interaction of coherent fields with randomly inhomogeneous media. This coherent light-matter interaction is a complex interference process leading to fields with strong fluctuations in intensity, fields that are most commonly known as speckle. A simple way to describe the intensity speckles is to consider the superposition of waves originating from discrete centers as a result of scattering. Different scattering regimes may vary from “single scattering” specific to most surface scattering to different degrees of multiple scattering characteristic to the interaction with three-dimensionally disordered media. When one single polarization component is analyzed, i.e. when the speckle field is measured through a polarizer, the intensity contrast often reaches unity. This is the case of the so-called fully developed speckle pattern, a manifestation of interference between a large numbers of wavelets with uniformly distributed random phases. This is a rather universal behavior present in scattering from a variety of media ranging from metallic rough surfaces to diffusive materials. However, the distribution of polarization states in REF is much richer and non-universal properties are to be expected. Most importantly, it is anticipated that the polarization properties of REF corresponding to different scatting regimes will depend greatly on the strength of the scattering process. For instance, it is likely that when the wave interaction is dominated by single scattering processes, a fully developed speckle pattern will occur but the REF polarization will strongly resemble the

incident state of polarization. On the other hand, when the interaction is subject to strong multiple scattering, the scattered field remains locally fully polarized but its state of polarization will vary from point to point. When the scattering process is completely diffusive, universal distributions emerge for the polarization parameters. It is therefore of interest to examine in detail the relation between the degree (order) of scattering and the polarization properties of the resulting REF.

Distribution Statement

This is block 12 on the SF298 form.

Distribution A - Approved for Public Release

Explanation for Distribution Statement

If this is not approved for public release, please provide a short explanation. E.g., contains proprietary information.

SF298 Form

Please attach your SF298 form. A blank SF298 can be found here. Please do not password protect or secure the PDF The maximum file size for an SF298 is 50MB.

SF 298.pdf

Upload the Report Document. File must be a PDF. Please do not password protect or secure the PDF . The maximum file size for the Report Document is 50MB.

Dogariu _Final REPORT _ AFOSR.pdf

Upload a Report Document, if any. The maximum file size for the Report Document is 50MB.

Archival Publications (published) during reporting period:

Changes in research objectives (if any):

Change in AFOSR Program Manager, if any:

Extensions granted or milestones slipped, if any:

AFOSR LRIR Number

LRIR Title

Reporting Period

Laboratory Task Manager

Program Officer

Research Objectives

Technical Summary

Funding Summary by Cost Category (by FY, $K)

	Starting FY	FY+1	FY+2
Salary			
Equipment/Facilities			
Supplies			
Total			

Report Document

Report Document - Text Analysis

Report Document - Text Analysis

Appendix Documents

2. Thank You

E-mail user

Jun 09, 2015 14:57:54 Success: Email Sent to: apotter@ucf.edu